https://doi.org/10.5194/egusphere-2026-6811
Preprint. Discussion started: 11 November 2026
© Author(s) 2026. CC BY 4.0 License.

Benthic cyanobacterial mats enhance nitrogen turnover in a eutrophic reservoir

Archana Venkatachari[1], Annie Bourbonnais[1], Kathryn L. Cottingham[2]

[1]School of the Earth, Ocean and Environment, University of South Carolina, Columbia, SC 29208, USA

[2]Department of Biological Sciences, Dartmouth College, Hanover, NH 03755, USA

Correspondence to: Annie Bourbonnais (abourbonnais@seoe.sc.edu)

Abstract. Benthic cyanobacterial mats are widespread in eutrophic lakes, but their effects on sediment phosphorus (P), iron (Fe), and nitrogen (N) cycling are poorly quantified. We studied *Microseira wollei*, a mat-forming cyanobacterium capable of N_2 fixation and toxin production, in Lake Wateree, South Carolina (USA). We sampled paired sites with and without mats at two locations in March and monthly from June through October 2023 (three dates per location), and measured P, Fe, and N concentrations in mat interstitial water and porewater, and N transformation rates and fluxes using ^{15}N-labelled and unlabelled whole-core incubations. Porewater P and nitrate (NO_3^-) were higher beneath benthic mats in June and July and Fe was higher in June, September, and October, whereas ammonium (NH_4^+) was lower beneath mats in June. Potential denitrification rates did not differ on average between paired sites (24.2 ± 13.9 vs. 19.3 ± 12.2 µmol N m^{-2} h^{-1} with and without mats), but increased with mat thickness (r^2 = 0.62). Potential dissimilatory nitrate reduction to ammonium (DNRA) rates, measured as $^{15}NH_4^+$ production from added $^{15}NO_3^-$, were 2.3 times higher in mat-covered sediments (13.1 ± 4.4 vs. 5.8 ± 3.3 µmol N m^{-2} h^{-1}) but remained smaller than denitrification, accounting on average for 39 % of total NO_3^- reduction in mat sediments and 29 % in bare sediments. The net N_2 flux in unamended mat cores was directed from the water column to the sediments in all ten cores (−23.9 ± 32.2 µmol N m^{-2} h^{-1}), suggesting that N_2 fixation likely exceeded denitrification beneath mats, although the mean was not significantly different from zero or from that in cores without mats. *M. wollei* mats are therefore hotspots of N turnover: they enhance denitrification with increasing mat thickness, more than double DNRA, may support N_2 fixation, and release P, Fe, and NH_4^+ from the sediments, complicating the management of eutrophic lakes.

https://doi.org/10.5194/egusphere-2026-6811
Preprint. Discussion started: 11 November 2026
© Author(s) 2026. CC BY 4.0 License.

1 Introduction

Harmful cyanobacterial blooms have become more widespread and frequent in lakes worldwide, driven by nutrient inputs (Paerl and Fulton, 2006) and by warming and other aspects of climate change (Paerl and Huisman, 2008). These blooms often produce potent toxins and volatile organic compounds that impair water quality and pose risks to human and animal health (Wood et al., 2020), at considerable economic cost (Dodds et al., 2009). Cyanobacterial blooms also contribute to primary production and influence nutrient cycling (Cottingham et al., 2015). Beyond pelagic blooms, benthic cyanobacterial mats, which play an important role in lake ecology (Vadeboncoeur et al., 2002), are comparatively understudied, yet they may also produce toxins (Wood et al., 2020). Cultural eutrophication generally shifts primary production from the benthos to the water column because pelagic blooms shade the sediment surface (Vadeboncoeur et al., 2003); however, shallow littoral zones of eutrophic lakes and reservoirs often remain within the photic zone and can support dense benthic mats that persist for years (Putnam et al., 2022; Crandell, 2024). Because these mats form distinct microenvironments, with steep redox gradients and rich microbial assemblages (Stal, 1995; Powell and McCoy, 2024), understanding their role in nutrient cycling is important for forecasting eutrophication trends and managing nutrient budgets in the lakes where they occur (Vadeboncoeur et al., 2002; Cottingham et al., 2015).

Phosphorus (P) and nitrogen (N) act differently in lake sediments and therefore require different management strategies. P has no significant gaseous phase; it is retained in sediments mainly by sorption to, and co-precipitation with, iron (Fe), aluminium, and calcium minerals, and it is released, together with dissolved Fe(II), when Fe(III) oxides are reduced under low-oxygen and anoxic conditions (Hupfer and Lewandowski, 2008) or when pH rises during intense photosynthesis (Jensen and Andersen, 1992). Benthic cyanobacterial mats can promote this release by adding labile organic carbon (OC) that fuels O_2 consumption and creates anoxia at the sediment surface (Crandell, 2024); at Lake Wateree, *M. wollei* growth is sustained by legacy sedimentary P (Putnam et al., 2022; Crandell, 2024). Whereas internal P loading is controlled largely by sediment redox chemistry (Hupfer and Lewandowski, 2008), internal N loading depends on the balance between microbial N removal and N recycling (Burgin and Hamilton, 2007; Paerl et al., 2016).

https://doi.org/10.5194/egusphere-2026-6811
Preprint. Discussion started: 11 November 2026
© Author(s) 2026. CC BY 4.0 License.

The dominant sedimentary N fluxes are microbially mediated transformations among dissolved nitrate (NO_3^-), nitrite (NO_2^-), ammonium (NH_4^+), and gaseous N (N_2) (Seitzinger, 1988; Gruber and Galloway, 2008). Denitrification converts NO_3^- and NO_2^- to N_2 (Seitzinger, 1988), and anaerobic ammonium oxidation (anammox) combines NO_2^- and NH_4^+ to form N_2 (Dalsgaard et al., 2005); both remove bioavailable N. Dissimilatory nitrate reduction to ammonium (DNRA) instead converts NO_3^- to NH_4^+, retaining N in a bioavailable form (Gardner et al., 2006; Burgin and Hamilton, 2007). The dominant pathway depends on the supply of electron donors relative to NO_3^- (Tiedje et al., 1983; Tiedje, 1988). High OC to NO_3^- ratios favour DNRA (Hardison et al., 2015), NO_3^--replete conditions with moderate OC favour denitrification (Burgin and Hamilton, 2007), and low OC together with NO_2^- availability favours anammox (Dalsgaard et al., 2005). Reduced iron (Fe(II)) (Robertson and Thamdrup, 2017; Rahman et al., 2019) and sulfide (Brunet and Garcia-Gil, 1996) can also serve as electron donors for DNRA, and temperature and oxygen control the seasonal dynamics of all three processes (Bonaglia et al., 2014).

Whether a lake remains N limited over timescales relevant to management depends on the balance between N inputs (external loading, N_2 fixation, and internal recycling) and N losses (denitrification, anammox, burial, and hydraulic export through outflows). Recent multi-year in-lake mesocosm experiments show that stopping N inputs while P loading continues can rapidly reduce phytoplankton biomass in shallow, P-rich lakes (Scott et al., 2025), and re-analysis of the multi-decadal Lake 227 record indicates that N_2 fixation does not fully compensate for reduced external N inputs over management-relevant timescales (Scott and McCarthy, 2010). Nevertheless, benthic N_2 fixation occurs simultaneously with denitrification in many sediments (Fulweiler et al., 2007; Rao and Charette, 2012), including at high dissolved inorganic N (DIN) concentrations (Gardner et al., 2006; Knapp, 2012; McCarthy et al., 2016), and can offset a substantial fraction of N losses on seasonal to annual timescales (McCarthy et al., 2016; Newell et al., 2016). Most N fixed by cyanobacteria becomes available to the wider community only with the remineralization of the N_2-fixing biomass, although exudation and cell lysis release some N sooner (Cottingham et al., 2015), so the fate and timing of release of the fixed N matter as much as the amount fixed (Scott and McCarthy, 2010), and net N_2 fluxes can switch between net fixation and net denitrification on daily to interannual timescales (Newell et al., 2016). The contribution of benthic cyanobacterial mats to the balance between N inputs and N losses remains poorly constrained.

https://doi.org/10.5194/egusphere-2026-6811
Preprint. Discussion started: 11 November 2026
© Author(s) 2026. CC BY 4.0 License.

Cyanobacteria influence sediment nutrient cycling via effects on sediment–water P dynamics and N_2 fixation and by altering environmental conditions at the sediment surface (Cottingham et al., 2015). Benthic mats fix carbon at high rates, and the heterotrophic degradation of this OC within and beneath the mat sustains their internal redox gradients (Powell and McCoy, 2024). Although they produce O_2 in the light, respiration of this OC in the dark creates steep O_2 gradients, so that anoxia develops within millimetres below the mat surface and throughout the night (Stal, 1995); these conditions favour N_2 fixation (Stal, 1988) and anaerobic NO_3^- reduction by denitrification and DNRA (Hardison et al., 2015; Jiang et al., 2020b). Mat productivity is strongly seasonal because the growth of mat-forming cyanobacteria is controlled by light and temperature (Stal, 1995); *Microseira wollei* mats accumulate biomass during the warm growing season (Putnam et al., 2022).

Microseira wollei (formerly *Lyngbya wollei*; McGregor and Sendall, 2015) has been studied since the 1990s primarily because it forms dense benthic mats that can produce potent toxins, which threaten drinking water and recreational resources (Yin et al., 1997; Lévesque et al., 2012; Poirier-Larabie et al., 2020). It is globally distributed and particularly well documented in the southeastern United States (Fig. S1). Its perennial mats have been linked to the release of sediment P (Putnam et al., 2022) and fix N_2 (Phlips et al., 1992). Whether its mats also promote denitrification and DNRA, as the anoxic conditions beneath cyanobacterial mats would predict (Stal, 1995), has not been tested, so whether the mats act, on balance, as internal sources or sinks of nutrients is unresolved; their role in nutrient cycling has received much less attention than their toxins.

The primary objective of this study was to examine the direct and indirect effects of *M. wollei* benthic mats on sediment nutrient cycling: directly, by mediating P and N transformations through microbial metabolic activity, and indirectly, by modifying sediment redox and pH conditions. We compared P, Fe, and N dynamics between sediments colonized by *M. wollei* mats and bare sediments at Lake Wateree, South Carolina, a reservoir with recurrent *M. wollei* proliferations for more than a decade (Putnam et al., 2022; Crandell, 2024), with a particular focus on the partitioning between N-removal and N-recycling processes. We used ^{15}N-labelled whole-core sediment incubations to quantify potential denitrification and DNRA rates and to test for the presence of anammox, and unlabelled control cores to quantify the net sediment–water N_2 flux. The ^{15}N-derived rates are potential rates: the tracer raises the NO_3^- concentration above

https://doi.org/10.5194/egusphere-2026-6811
Preprint. Discussion started: 11 November 2026
© Author(s) 2026. CC BY 4.0 License.

ambient and the incubations were run at a single temperature, so the rates compare the capacity of sediments with and without mats for each process but are not in situ fluxes (Sect. 2.3.2). We measured porewater concentrations of phosphate (PO_4^{3-}), NO_3^-, NO_2^-, NH_4^+, and total dissolved Fe, and sediment characteristics in a different set of cores. We anticipated that *M. wollei* mats would enhance the remobilization of sedimentary P and Fe and would increase denitrification by supplying labile OC and consuming O_2. We also predicted that N recycling by DNRA relative to N loss by denitrification would be more pronounced at sites with mats than at bare sites, because the mats supply labile OC and Fe(II) and deplete NO_3^-, raising the ratio of electron donors to NO_3^-. Our study focuses on the growing season, when mat effects on nutrient cycling are expected to be largest, and we interpret the balance between N removal and N recycling over seasonal timescales rather than over the multi-year timescales relevant to burial.

2 Methods

2.1 Study site and sampling

Lake Wateree is a hydroelectric reservoir on the Catawba–Wateree River in Kershaw, Fairfield, and Lancaster counties, South Carolina (USA). It has a surface area of 55 km^2 and a mean depth of 7 m (Stachelek et al., 2018), a hydraulic residence time of about 27 d (Tufford et al., 2012; Putnam et al., 2022), summer water temperatures that exceed 30 °C (WaterWatch, 2025), and recurrent *M. wollei* proliferations along its shoreline, where it grows in the photic zone at water depths of less than about 2 m (Putnam et al., 2022). A shoreline survey in spring 2025 indicated that roughly a third to a half of the shoreline was affected by benthic mats (Fig. S2); in earlier grab samples of the mats, *M. wollei* accounted for about half (53 %) of the 16S ribosomal RNA gene sequences (Putnam et al., 2022). These dense mats, often entangled with leaf litter and dead biomass, extend up to 4 m from the shoreline into the lake. *M. wollei* proliferates on sedimentary P at Lake Wateree (Putnam et al., 2022), and more than 60 % of the sediment P cycles with reducible Fe phases (Crandell, 2024).

We established paired sampling sites near the inflows of Dutchman Creek and Colonel Creek (Fig. 1). Within each pair, one site was colonized by *M. wollei*-dominated benthic mats and the other, about 1 km (Dutchman Creek) and 4 km (Colonel Creek) away along the same shoreline, lacked mats (hereafter the mat sites and the bare sites). Sites were selected based on prior knowledge of *M. wollei* occurrence and on shoreline access from land. Because logistics

https://doi.org/10.5194/egusphere-2026-6811
Preprint. Discussion started: 11 November 2026
© Author(s) 2026. CC BY 4.0 License.

precluded sampling both locations on the same date, the two locations were sampled in different months: Dutchman Creek in March, June, and September and Colonel Creek in July, August, and October 2023, so that each pair of sites was sampled three times.

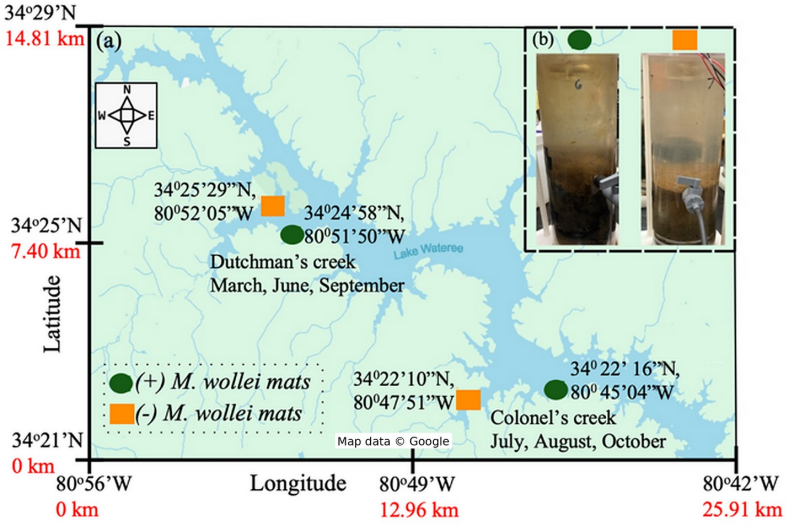


Figure 1. (a) Sampling locations at Lake Wateree, South Carolina, showing the paired sites with (green circles) and without (orange squares) *M. wollei* benthic mats near the inflows of Dutchman Creek and Colonel Creek (base map: Google Maps, map data © Google). (b) Example sediment cores with (left) and without (right) a benthic mat; the mat is the dark, filamentous layer at the top of the sediment in the left core (a labelled close-up of a mat core is shown in Fig. S3).

On each sampling date we collected 10–12 whole sediment cores per site at approximately 1 m water depth using a push corer fitted with acrylic core tubes (9.5 cm inner diameter, 40 cm length; Fig. 2). Each core contained sediment (including the mat, when present) overlain by 8–27 cm of site water. Cores from the mat sites (hereafter mat cores) generally contained more sediment, and therefore less overlying water (mean 13 cm), than cores from the bare sites (bare cores; mean 20 cm). Cores were capped at both ends without headspace, kept upright in the dark in insulated coolers at ambient temperature, and transported to the laboratory within 3 h of collection. We also collected 60 L of overlying site water at each site before coring, transferring it with clean 2 L graduated cylinders into 20 L cubitainers; in the laboratory this water was stored at room temperature in 1 L plastic cubitainers and used to replace the water withdrawn from the cores during the incubations.

https://doi.org/10.5194/egusphere-2026-6811
Preprint. Discussion started: 11 November 2026
© Author(s) 2026. CC BY 4.0 License.

In the laboratory, the cores were used for ^{15}N-tracer experiments with ^{15}N-labelled NO_3^- or NH_4^+ and for unlabelled controls (Sect. 2.3), and for porewater sampling and characterization of sediment properties (grain size, porosity, %C, %N) and cyanobacterial mat thickness (Sect. 2.2). All cores were acclimatized for 24 h in the laboratory at 16–17 °C before treatments began; the light conditions of each treatment are described in Sects. 2.2 and 2.3.1. Because incubations were run at 16–17 °C in all months, seasonal differences in rates reflect differences in sediment properties and microbial communities at a common temperature rather than in situ temperature.

2.2 Porewater sampling and sediment characteristics

We collected porewater and sediment samples from four cores per site on each sampling date. Duplicate cores from each site were first held for 24 h under either light or dark conditions to distinguish daytime from night-time conditions in the mat interstitial water and sediment porewater. The light treatment used a 200 W growth lamp that produced 90–120 µmol photons m^{-2} s^{-1} at the sediment–water interface, as measured with a photosynthetically active radiation (PAR) meter (Apogee Instruments, UT, USA); the dark treatment was achieved by covering the cores with a black plastic box.

After 24 h, porewater was extracted using Rhizon samplers (2.5 mm outer diameter, nominal membrane pore size 0.15 µm; Rhizosphere Research Products, Wageningen, the Netherlands) inserted horizontally through pre-drilled, sealed ports at the sediment–water interface (0 cm) and at 1, 2, or 3 cm intervals to a depth of 7–10 cm. The deepest port depended on the sediment height and on whether the Rhizon could be inserted, given the sediment texture and porosity. We withdrew 5 mL of porewater per depth using evacuated syringes, which was sufficient for inorganic nutrients only; dissolved organic N and P could not be measured. This volume is 8–10 % of the porewater in a 1 cm sediment interval at the mat sites (porosity 0.74–0.87) and about 19 % at the bare sites (porosity 0.36–0.38; Table S1), which limits the drawing of porewater from adjacent depth intervals (Seeberg-Elverfeldt et al., 2005). Porewater was filtered in line by the Rhizon membrane at the moment of collection, so microbial activity in the sample after collection was minimal. Samples were frozen (−20 °C) until analysis of PO_4^{3-}, NO_3^-, NO_2^-, NH_4^+, and total dissolved Fe using standard colorimetric methods (Grasshoff et al., 1999) adapted for a SEAL AQ300 discrete analyser (SEAL Analytical, WI, USA). Values below the method detection limit, including negative readings, were set to zero (25 of 1460 values).

https://doi.org/10.5194/egusphere-2026-6811
Preprint. Discussion started: 11 November 2026
© Author(s) 2026. CC BY 4.0 License.

After porewater collection, we measured the cyanobacterial mat thickness in each core with a metric ruler placed along the outside of the core tube, distinguishing the mat from the underlying sediment by colour and texture (Fig. S3). We used thickness rather than biomass because the mats contained leaf litter, twigs, live snails, and snail shells that precluded a reliable biomass estimate. Cores were then extruded and the top 1 cm was sliced. The sliced sediment was weighed before and after drying overnight at 40 °C to estimate porosity (the volume of water lost on drying, taken as 1 mL g^{-1}, divided by the sample volume) and wet bulk density (wet mass divided by the sample volume; Ullman and Aller, 1982), and the dried sediment was sieved through a nested stack of 3.35, 2.00, 1.00, 0.50, 0.125, and 0.063 mm sieves to determine the median grain size. Sediment %C and %N (total C and N; the samples were not acidified) were measured on triplicate subsamples from the top 1 cm of each core with a PyroCube elemental analyser (Elementar Americas Inc., NY, USA; Meyers and Teranes, 2001). The triplicate subsamples and the four cores were averaged per site and sampling date. The mat thickness used in the rate regressions (Sect. 3.4) is that recorded for each incubated core (Sect. 2.3.1).

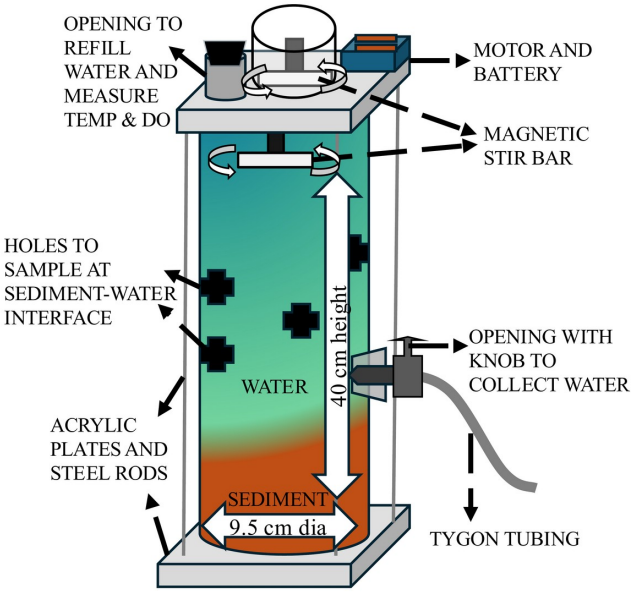
2.3 ^{15}N-tracer whole-core incubations

2.3.1 Design and sample collection

We used the remaining cores from each site on each sampling date to estimate N-cycling rates with the isotope pairing technique (IPT; Nielsen, 1992) and with N_2:Ar measurements in unamended cores (Kana et al., 1994; Fulweiler and Nixon, 2012). The heights of the overlying water, sediment, and benthic mat (when present) were recorded for each core. The cores were then sealed with acrylic lids and the overlying water (not the sediment) was stirred continuously at 30 rotations per minute with a magnetic stir bar suspended from the lid (Fig. 2), a rate that kept the water mixed without resuspending sediment. The incubations were run under ambient room light (Sect. 2.2). After the 24 h acclimatization period, either $Na^{15}NO_3$ (98 atom % ^{15}N) or $^{15}NH_4Cl$ (99 atom % ^{15}N; Cambridge Isotope Laboratories, MA, USA) was injected into the overlying water just above the sediment–water interface of two or three cores per site for $^{15}NO_3^-$ and of one core per site for $^{15}NH_4^+$ (two in June). The tracer was injected with a 21 G × 120 mm needle attached to a 1 or 3 mL syringe; the final added concentration was 50 µmol N L^{-1} (0.7 mg N L^{-1}). Two additional control cores per site received no tracer. Ambient NO_3^- in the overlying water was 44–96 µmol L^{-1} (monthly means; Table S1), therefore the ^{15}N atom fraction of the overlying-water NO_3^- pool after tracer addition was approximately 34–53 % (0.29–0.61 for

https://doi.org/10.5194/egusphere-2026-6811
Preprint. Discussion started: 11 November 2026
© Author(s) 2026. CC BY 4.0 License.

232 individual cores; Sect. S1.3). Ambient NH_4^+ was 0–66 µmol L^{-1} (Table S1), therefore the ^{15}N
233 atom fraction of the NH_4^+ pool after tracer addition was approximately 43–99 %.



234
235 **Figure 2.** Core set-up for the ^{15}N-tracer and control incubations: the overlying water was stirred with a magnetic stir
236 bar suspended from the lid, and samples were withdrawn through a spigot at the sediment–water interface.

237 Overlying water was sampled at the sediment–water interface seven times, every 12 h for 72 h
238 starting from the time of tracer addition, through a spigot with a turn valve connected to Tygon
239 tubing (Fig. 2). Samples for dissolved gases ($^{28}N_2$, $^{29}N_2$, $^{30}N_2$, and ^{40}Ar) were collected in triplicate
240 by overflowing 12 mL glass Exetainers (Labco, UK) by at least two volumes, preserved with 50
241 µL of saturated $HgCl_2$ solution, capped without headspace, and stored submerged in water at
242 room temperature until analysis within 3 d. Samples for $^{15}NH_4^+$ (DNRA) and for nutrient
243 concentrations were taken from the same withdrawn water at each time point and frozen (−20
244 °C) until analysis (Sect. 2.3.2; nutrients as in Sect. 2.2). Nutrient samples from the incubations
245 were not filtered before freezing; the reported concentrations therefore reflect the net balance of
246 microbial processes occurring in the sample between collection and freezing, which can alter
247 NH_4^+ and PO_4^{3-} concentrations in unfiltered samples (Reed et al., 2023). Because samples were
248 frozen within 10 min of collection, we expect these changes to be small.

249 At each time point, including the start of the incubation, we measured dissolved O_2 and
250 temperature in the overlying water of every incubated core, including the $^{15}NH_4^+$-amended cores,

https://doi.org/10.5194/egusphere-2026-6811
Preprint. Discussion started: 11 November 2026
© Author(s) 2026. CC BY 4.0 License.

with a luminescent dissolved oxygen probe (Hach, CO, USA), to document the O_2 conditions under which the rates were measured and to calculate dissolved gas concentrations at equilibrium. The dissolved O_2 record of all incubated cores is reported in Fig. S4 and Table S2 and summarized in Sect. 3.3. After each sampling, the volume of water withdrawn was recorded to account for dilution of dissolved $^{28}N_2$, $^{29}N_2$, and $^{30}N_2$, and each core was refilled with site water (containing the same ^{15}N tracer concentration for amended cores, or no tracer for controls) while ensuring that no air was entrapped, and resealed. The replacement water was bubbled with air before use and, as its N_2:Ar ratio was not measured, treated as air-equilibrated in the flux calculations (Sect. S1.1); the overlying water of the cores remained oxic throughout the incubations (Sect. 3.3).

2.3.2 Analytical methods and rate calculations

Dissolved $^{28}N_2$, $^{29}N_2$, $^{30}N_2$, and ^{40}Ar concentrations were measured with a membrane inlet mass spectrometer (MIMS; Bay Instruments, MD, USA) following Kana et al. (1994) and Eyre et al. (2002). Triplicate measurements were averaged before rates were calculated. Air-equilibrated freshwater standards at 10 and 20 °C were used to calibrate the N_2 and Ar signals; the air-equilibrium N_2 and Ar concentrations at the measured incubation temperature were calculated with the solubility equations of Hamme and Emerson (2004).

Potential denitrification rates were calculated with the IPT from the linear increase in $^{29}N_2$ and $^{30}N_2$ over time in cores amended with $Na^{15}NO_3$ (Nielsen, 1992; Eyre et al., 2002). The IPT assumes that $^{29}N_2$ and $^{30}N_2$ are produced by random pairing of ^{14}N and ^{15}N within a single NO_3^- pool in the denitrification zone and that anammox contributes negligibly to N_2 production (Risgaard-Petersen et al., 2003). Because anammox was below detection in all $^{15}NH_4^+$-amended cores (Sect. 3.4), the anammox assumption of the original IPT was met; at a site where anammox contributed 6 % of N_2 production, the IPT overestimated total N_2 production by only 2.5 % (Risgaard-Petersen et al., 2003). Before the slopes were calculated, the $^{29}N_2$:$^{28}N_2$ and $^{30}N_2$:$^{28}N_2$ ratios were corrected for the replacement of the sampled water with site water containing N_2 at natural isotopic abundance; the correction was applied to the ^{15}N excess over natural abundance for the water replaced after the previous sampling (Sect. S1.1). Because the tracer addition increased the overlying-water NO_3^- concentration by about 50–115 %, all ^{15}N-derived rates are reported as potential rates.

https://doi.org/10.5194/egusphere-2026-6811
Preprint. Discussion started: 11 November 2026
© Author(s) 2026. CC BY 4.0 License.

Anammox was tested from the increase in $^{29}N_2$ in cores amended with $^{15}NH_4Cl$ (Song et al., 2016). These cores were incubated in the same way as the $^{15}NO_3^-$-amended cores, with the overlying water remaining oxic (38–265 µmol O_2 L^{-1}; Fig. S4), so some added $^{15}NH_4^+$ could in principle have been nitrified to $^{15}NO_2^-$/$^{15}NO_3^-$ and then denitrified together with ambient $^{14}NO_3^-$, also producing $^{29}N_2$; the $^{29}N_2$ production in these cores therefore includes any such coupled nitrification–denitrification as well as anammox. It was below the method detection limit (approximately 1.1 µmol N m^{-2} h^{-1}, calculated from three standard deviations of the $^{29}N_2$:$^{28}N_2$ ratio of replicate unlabelled standards; Sect. S1.4) in all cores, so anammox was not detected.

Potential DNRA was quantified as the production of $^{15}NH_4^+$ from the added $^{15}NO_3^-$ in the same cores used for denitrification, by hypobromite oxidation of NH_4^+ to N_2 followed by MIMS analysis (OX/MIMS; Yin et al., 2014). Samples were frozen (−20 °C) without acidification and stored for 12–20 months before analysis (Sect. S1.3). After thawing, each sample was purged with high-purity N_2, which strips the dissolved gases (including any $^{29}N_2$ and $^{30}N_2$ produced by denitrification during the incubation) and replaces them with N_2 at natural isotopic abundance, so that the ^{15}N excess measured after oxidation derives only from NH_4^+. Alkaline hypobromite iodine solution was then injected to oxidize NH_4^+ to N_2, and $^{28}N_2$, $^{29}N_2$, and $^{30}N_2$ were measured by MIMS. The ^{15}N in the gas, $[^{15}N]_{gas} = [^{29}N_2] + 2\,[^{30}N_2]$, was converted to the $^{15}NH_4^+$ concentration by linear calibration against NH_4Cl standards containing 0–20 % ^{15}N that were purged, oxidized, and analysed in the same way as the samples (r^2 = 0.99). The method detection limit, defined as three standard deviations of the unlabelled standards, was 0.6 µmol $^{15}NH_4^+$ L^{-1}. The analytical batches, the drift and background corrections, and the calibration are detailed in Sect. S1.3.

The potential DNRA rate was calculated from the areal production rate of $^{15}NH_4^+$ (the slope of the $^{15}NH_4^+$ produced versus incubation time, corrected for the dilution by the water replaced at each time point (Sect. S1.1), multiplied by the height of the overlying water; Gardner et al., 2006; McCarthy et al., 2016) divided by the ^{15}N atom fraction of the overlying-water NO_3^- pool after tracer addition (0.29–0.61; Sect. S1.3), which scales the $^{15}NH_4^+$ production to the whole NO_3^- pool (Risgaard-Petersen and Rysgaard, 1995; Dong et al., 2009). The share of DNRA in NO_3^- reduction was calculated as DNRA / (DNRA + total denitrification). Because the rates are based on the $^{15}NH_4^+$ recovered in the overlying water, any $^{15}NH_4^+$ that was assimilated or nitrified

https://doi.org/10.5194/egusphere-2026-6811
Preprint. Discussion started: 11 November 2026
© Author(s) 2026. CC BY 4.0 License.

within the mat, or retained in the sediment, is not included, therefore the rates may be underestimated.

The net sediment–water N_2 flux was determined from the change in the N_2:Ar ratio over the 72 h incubation in the control cores without tracer addition (Kana et al., 1994; Fulweiler and Nixon, 2012). A positive net flux (from the sediment to the water column) indicates net N_2 production (denitrification plus anammox exceeding N_2 fixation), and a negative net flux (from the water column to the sediment) indicates net N_2 consumption (N_2 fixation exceeding denitrification). To allow direct comparison among processes, all rates, including net N_2 fluxes, are reported in µmol N m^{-2} h^{-1}. Rates were calculated from the measured height of the overlying water in each core; all equations are given in Sect. S1 of the Supplement.

2.4 Statistical analyses

All analyses were carried out in R (version 4.3.3; R Core Team, 2024); the scripts and data files are available in the data repository (see Code and data availability). The data from March were excluded from all statistical analyses because the water level during that month was about 1 m higher than in the other months due to construction work at the Lake Wateree dam. The March data are reported in Table S1 for completeness. Assumptions of normality and homogeneity of variance were assessed with residual plots. All tests were two-tailed. We report effect sizes with 95 % confidence intervals (CI) together with the test statistics throughout.

Depth-integrated porewater nutrient concentrations were calculated for each core as the area under the concentration–depth profile (trapezoidal integration, mg L^{-1} cm) over the 0–2 cm interval below the sediment–water interface (0–1 cm in August; the green bands in Fig. 3), chosen to encompass the mat horizon of the mat cores; the same interval was used in bare cores. Because location and month are confounded in the paired design (Sect. 2.1), we did not test for temporal trends or month × mat interactions. Within each month, we fitted a two-way analysis of variance model (Type III sums of squares) with mat presence, light condition (light vs. dark), and their interaction as fixed factors (Table S3). Each cell of these models contains two cores, which are subsamples of the single mat site and single bare site sampled in that month (Sect. 2.1); the tests therefore compare the two sites of a month, have low power, and detect only consistent differences between duplicate cores. These month-specific tests form a family of five tests per

https://doi.org/10.5194/egusphere-2026-6811
Preprint. Discussion started: 11 November 2026
© Author(s) 2026. CC BY 4.0 License.

response variable and factor, so we report Holm-adjusted *p*-values (Holm, 1979) and use adjusted $p \leq 0.05$ as the criterion for an effect.

For the N-cycling rates and the initial overlying-water nutrient concentrations, the primary test of the mat effect was a one-sample *t*-test on the five monthly mean differences (with minus without mats; Table S4); month is the pairing unit, so this test accounts for the changes in locations across months. As a secondary, exploratory analysis, we also report unequal-variance two-sample *t*-tests for each month separately, again with Holm-adjusted *p*-values (Table S5). To compare N removal with N recycling, we used a one-sample *t*-test on the within-core difference (total denitrification minus DNRA) for cores amended with $Na^{15}NO_3$, separately for cores with and without mats. Relationships between rates and the initial overlying-water concentrations of NH_4^+, NO_2^-, and NO_3^- were evaluated with Spearman's rank correlation (ρ) and Pearson's correlations (Table S6). We regressed potential denitrification and potential DNRA against mat thickness by ordinary least squares for the mat cores, and repeated the regression on the five monthly means; as a sensitivity analysis, the regression was also refitted five times, each time omitting one month. Finally, we tested whether the mean monthly net N_2 flux of the mat cores differed from zero with a one-sample *t*-test.

3 Results

3.1 Field observations and sediment characteristics

In the field, the abundance and structure of *M. wollei* mats varied seasonally: thick floating mats were present in summer, which facilitated identifying the location of the benthic mats. In spring and autumn floating mats were absent, but benthic mats were always present at the mat sites. Mat thickness in the incubated cores averaged 0.8 ± 0.4 cm in June, 2.7 ± 0.3 cm in July, 1.0 ± 0.2 cm in August, 1.6 ± 0.5 cm in September, and 1.5 ± 0.3 cm in October (3.2 ± 0.8 cm in March; Table S1). Sediments at mat sites were finer (grain size 0.063 mm vs. 0.125–1 mm), more porous (0.74–0.87 vs. 0.36–0.38), and richer in C and N (0.75–4.50 % total C and 0.08–0.75 % N vs. 0.18–1.92 % C and 0.02–0.17 % N) than at bare sites (Table S1). Within-month standard deviations of %C and %N at mat sites were often as large as the means, indicating strong small-scale heterogeneity among replicate cores; %C at mat sites showed no consistent seasonal pattern (highest in June and October, 4.5 % and 3.6 %; lowest in August and September, 0.8–0.9 %; Table S1).

https://doi.org/10.5194/egusphere-2026-6811
Preprint. Discussion started: 11 November 2026
© Author(s) 2026. CC BY 4.0 License.

3.2 Porewater nutrient profiles

The effects of *M. wollei* mats on porewater nutrients differed among sampling months (Fig. 3; Table S3), whereas the effects of light and of the light × mat interaction were weak. After Holm adjustment, the only light effect was on porewater NO_2^- concentration in August ($F_{1,4}$ = 26.7, adjusted p = 0.033) and no interaction term had an adjusted $p \leq 0.05$ (Fig. S5; Table S3).

Depth-integrated porewater PO_4^{3-} concentration was higher in the presence of mats in June ($F_{1,4}$ = 22 785, adjusted $p < 0.001$) and July ($F_{1,4}$ = 80.9, adjusted p = 0.003) but not from August to October (Fig. 3d). Porewater NO_3^- concentration was higher with mats in June ($F_{1,4}$ = 30.6, adjusted p = 0.021) and July ($F_{1,4}$ = 48.8, adjusted p = 0.011; Fig. 3c), and NH_4^+ concentration was lower with mats in June ($F_{1,4}$ = 51.1, adjusted p = 0.010; Fig. 3a) and did not differ in the other months. Mats had no detectable effect on porewater NO_2^- concentration in any month after adjustment (adjusted $p \geq 0.116$; Fig. 3b). Total porewater dissolved Fe concentration was higher within mats in June ($F_{1,4}$ = 20.9, adjusted p = 0.031), September ($F_{1,4}$ = 322, adjusted $p < 0.001$) and October ($F_{1,4}$ = 181, adjusted $p < 0.001$; Fig. 3e).

https://doi.org/10.5194/egusphere-2026-6811
Preprint. Discussion started: 11 November 2026
© Author(s) 2026. CC BY 4.0 License.

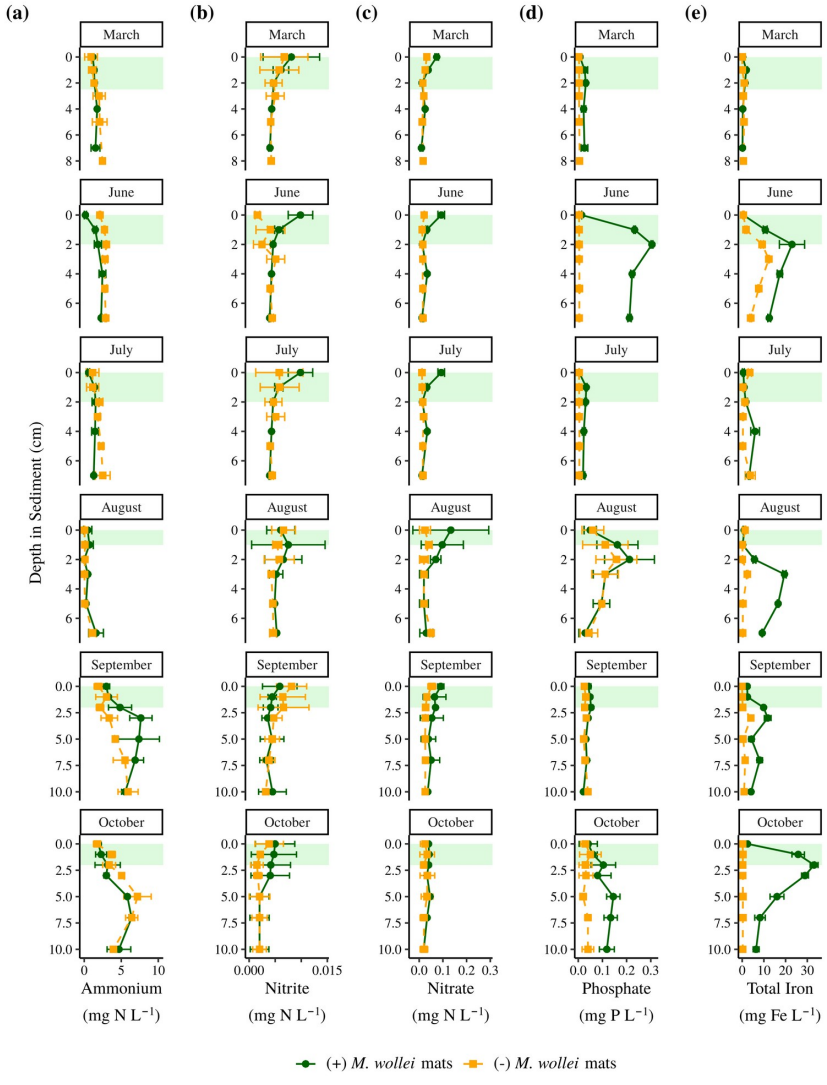


Figure 3. Porewater nutrient concentration profiles in cores with (green circles, solid lines) and without (orange squares, dashed lines) *M. wollei* benthic mats: (a) NH_4^+, (b) NO_2^-, (c) NO_3^-, (d) PO_4^{3-} and (e) total dissolved Fe. Points are means of all four cores (light and dark treatments), and error bars are standard deviations. Green bands mark the depth interval used for the depth-integrated statistics (Table S3): 0–2 cm below the sediment–water interface (0–1 cm in August), showing the mat horizon; March, which is excluded from the statistics, is shaded to 2.5 cm. See Fig. S5 for the light and dark treatments separately.

3.3 Dissolved oxygen during the incubations

Dissolved O_2 in the overlying water at the start of the incubations (all ^{15}N-amended and control cores) averaged 167 ± 60 µmol L^{-1} (5.4 ± 1.9 mg L^{-1}) in mat cores and 215 ± 45 µmol L^{-1} (6.9 ±

https://doi.org/10.5194/egusphere-2026-6811
Preprint. Discussion started: 11 November 2026
© Author(s) 2026. CC BY 4.0 License.

1.4 mg L^{-1}) in bare cores (June–October; Fig. S4; Table S2). O_2 generally declined over the 72 h incubations, to 143 ± 35 µmol L^{-1} in mat cores and 184 ± 36 µmol L^{-1} in cores without mats. In July, O_2, however, increased over time in the mat cores, likely due to net photosynthesis. The overlying water of these cores remained oxic throughout the incubations: the lowest O_2 value recorded was 38 µmol L^{-1} (1.2 mg L^{-1}), and only six of the 377 readings from June to October, all in mat cores, fell below the hypoxia level (62.5 µmol L^{-1} or 2 mg L^{-1}). The rates reported below were therefore measured under oxic conditions. O_2 was on average about 50 µmol L^{-1} lower in the presence of mats than in bare sediments (mean O_2 of each core over the incubation, averaged by month: mean monthly difference −48 µmol L^{-1}, 95 % CI −72 to −24; paired t_4 = −5.55, p = 0.005).

3.4 Potential N-cycling rates and net N_2 fluxes

Potential denitrification rates did not differ significantly between mat cores (24.2 ± 13.9 µmol N m^{-2} h^{-1}, mean ± standard deviation (SD); n = 13) and bare cores (19.3 ± 12.2 µmol N m^{-2} h^{-1}; n = 12) when averaged over the growing season (Fig. 4a). The mean of the five monthly differences was 3.5 µmol N m^{-2} h^{-1} (95 % CI −10.3 to 17.4; paired t_4 = 0.71, p = 0.52; Table S4), and no month-specific difference had an adjusted $p \leq 0.05$ (Table S5). In mat cores, however, potential denitrification rates increased linearly with mat thickness (Fig. 5a; slope 14.4 µmol N m^{-2} h^{-1} per cm of mat, 95 % CI 6.8–21.9; r^2 = 0.62); the relationship persisted when any one month was left out (slopes 12–26 µmol N m^{-2} h^{-1} per cm, all with 95 % CIs excluding zero). The slope on the five monthly means was similar (14.9 µmol N m^{-2} h^{-1} per cm, 95 % CI −2.7 to 32.6; r^2 = 0.71), and the relationship was positive within each location separately, although within a location thickness varied mainly between months (Dutchman Creek: slope 21 µmol N m^{-2} h^{-1} per cm, 95 % CI 1–42, r^2 = 0.79, n = 5; Colonel Creek: slope 12 µmol N m^{-2} h^{-1} per cm, 95 % CI 0.3–24, r^2 = 0.51, n = 8). Denitrification rates in mat cores were lowest in the two months with the thinnest mats (June: 4.6 ± 0.9 µmol N m^{-2} h^{-1}; August: 10.5 ± 2.6 µmol N m^{-2} h^{-1}); in August, the rate in mats was lower than in bare sediment (24.6 ± 11.4 µmol N m^{-2} h^{-1}). Conversely, denitrification rates were highest in the months with thicker mats (July: 34.5 ± 13.8 µmol N m^{-2} h^{-1}; September: 27.9 ± 6.9 µmol N m^{-2} h^{-1}; October: 32.3 ± 8.3 µmol N m^{-2} h^{-1}), exceeding the rates measured in bare sediment (Table S1). Potential denitrification rates were not correlated with the initial NH_4^+, NO_2^-, or NO_3^- concentrations in the overlying water ($|\rho| \leq 0.22$, $p \geq 0.30$; Table S6). The time

https://doi.org/10.5194/egusphere-2026-6811
Preprint. Discussion started: 11 November 2026
© Author(s) 2026. CC BY 4.0 License.

series of every core (isotope ratios for ^{15}N-labelled treatments, N_2:Ar for control cores, and $^{15}NH_4^+$ produced for DNRA rate measurements) are shown in Figs. S6–S8.

Potential DNRA rates, measured as $^{15}NH_4^+$ production and scaled to the whole NO_3^- pool (Sect. 2.3.2), were 2.3 times higher in mat cores (13.1 ± 4.4 µmol N m^{-2} h^{-1}) than in bare cores (5.8 ± 3.3 µmol N m^{-2} h^{-1}; Fig. 4b); the unscaled $^{15}NH_4^+$ production rates were 6.2 ± 2.2 and 2.7 ± 1.8 µmol N m^{-2} h^{-1} (Table S1). The mean monthly difference was 6.9 µmol N m^{-2} h^{-1} (95 % CI 0.9–13.0; paired $t_4 = 3.17$, $p = 0.034$; Table S4). Potential DNRA rates were higher in mat cores in four of the five growing-season months and similar in June (Table S1); the July, August, and October differences remained significant after Holm adjustment (adjusted $p = 0.026$, 0.026, and 0.017; September: adjusted $p = 0.18$; Table S5). $^{15}NH_4^+$ increased over time ($p < 0.05$) in 16 of the 25 cores. The method detection limit of $^{15}NH_4^+$ (three standard deviations of the unlabelled standards; Sect. 2.3.2; Yin et al., 2014) corresponds to a $^{15}NH_4^+$ production of 0.7–2.2 µmol N m^{-2} h^{-1} over the 72 h incubations; five of the 12 bare cores were at or below it. Potential DNRA rates increased with mat thickness (Fig. 5b; slope 2.5 µmol N m^{-2} h^{-1} per cm of mat, 95 % CI −0.9 to 5.9; $r^2 = 0.19$), but the relationship was much weaker than that observed for potential denitrification rates, and its 95 % CI included zero unless August was left out (leave-one-month-out slopes 0.5–4.0 µmol N m^{-2} h^{-1} per cm). Potential DNRA rates were positively correlated with the initial NH_4^+ concentration in the overlying water ($\rho = 0.63$, $p < 0.001$) but not significantly with the initial NO_2^- ($\rho = -0.21$, $p = 0.31$) or NO_3^- concentrations ($\rho = -0.25$, $p = 0.22$; Table S6). Initial NH_4^+ concentrations were consistently higher at the mat sites (monthly means 46–66 vs. 0–39 µmol L^{-1}; mean difference 46 µmol L^{-1}, 95 % CI 27–64; paired $t_4 = 6.85$, $p = 0.002$; Tables S1 and S4, where concentrations are given in mg N L^{-1}). Initial NO_2^- concentrations were slightly lower at the mat sites (mean difference −0.20 µmol L^{-1}, 95 % CI −0.36 to −0.03; paired $t_4 = -3.36$, $p = 0.028$), and initial NO_3^- concentrations did not differ between site types (Table S4).

Denitrification was the larger NO_3^- reduction pathway in both the presence and absence of cyanobacterial benthic mats. Total potential denitrification rates exceeded potential DNRA rates by 11.0 µmol N m^{-2} h^{-1} in mat cores (95 % CI 3.7–18.4; paired $t_{12} = 3.26$, $p = 0.007$) and by 13.5 µmol N m^{-2} h^{-1} in bare cores (95 % CI 6.2–20.7; paired $t_{11} = 4.08$, $p = 0.002$). DNRA accounted on average for 39 % (range 26–67 %) of total NO_3^- reduction (DNRA plus denitrification) in the

https://doi.org/10.5194/egusphere-2026-6811
Preprint. Discussion started: 11 November 2026
© Author(s) 2026. CC BY 4.0 License.

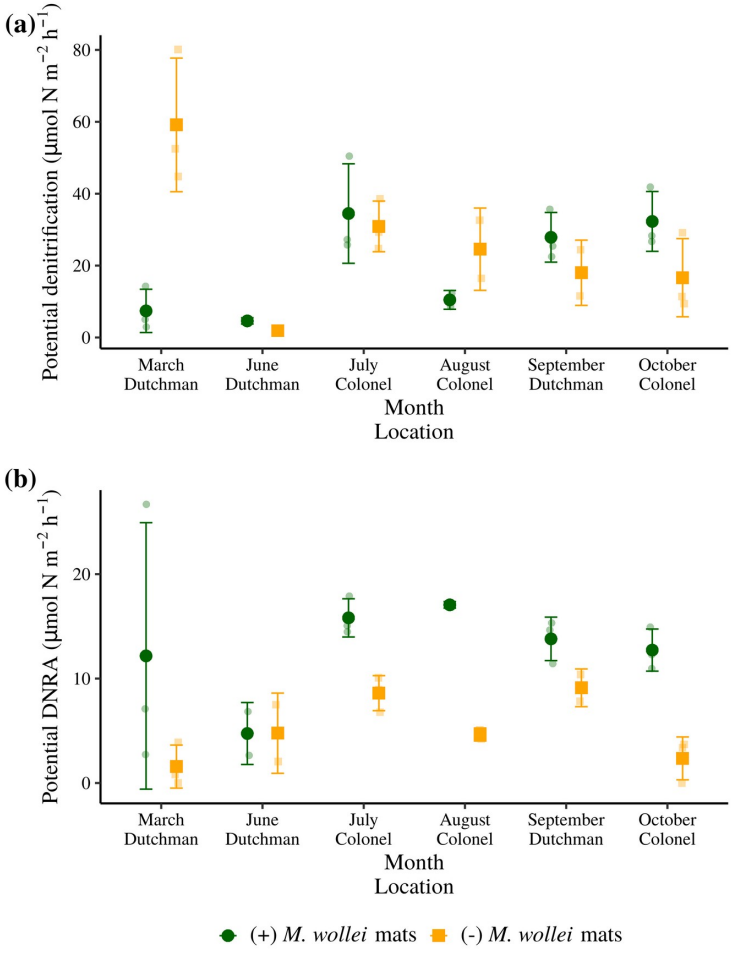
presence of mats and for 29 % (0–74 %) without mats; in one October bare core $^{15}NH_4^+$ did not increase and the DNRA rate was set to zero.

NH_4^+ accumulated in the overlying water of both core types during the ^{15}N incubations (Table S1). Converted to areal rates by taking into account the water height of each core (8–26 cm in these cores), the accumulation of 0.17–0.37 µmol NH_4^+ L^{-1} h^{-1} in mat cores (monthly means) corresponds to an NH_4^+ efflux of roughly 15–60 µmol N m^{-2} h^{-1}, and that in bare cores to an efflux of 7–42 µmol N m^{-2} h^{-1}. However, these values should be interpreted with caution as the samples were unfiltered (Sect. 2.3.1).

Production of $^{29}N_2$ in cores amended with $^{15}NH_4^+$ was below the method detection limit at all sites and in all months, so anammox was not detected. Therefore, denitrification was the only N-removal pathway measured in this study.

In the unamended control cores, the net N_2 flux during the growing season averaged −23.9 ± 32.2 µmol N m^{-2} h^{-1} in mat cores (n = 10), i.e. a net flux from the water column into the sediment (net N_2 uptake), and +0.8 ± 34.0 µmol N m^{-2} h^{-1} in bare cores (n = 10; Fig. 6). The net N_2 flux was directed into the sediment in all ten mat cores in every growing-season month (monthly means −59.8 to −2.4 µmol N m^{-2} h^{-1}; Table S1). In bare cores, the net N_2 flux was directed from the sediment to the water column, suggesting net N_2 production from benthic denitrification, in June, July, and October. However, in August and September in bare cores, the net N_2 flux reversed and was directed from the water column into the sediment, indicating the dominance of N_2 fixation. The mean of the five monthly means in mat cores did not differ significantly from zero (one-sample t_4 = −2.14, p = 0.10). The mean monthly difference in net N_2 flux between mat and bare cores was −24.7 µmol N m^{-2} h^{-1} (95 % CI −85.5 to 36.1; paired t_4 = −1.13, p = 0.32; Table S4). The month-specific 95 % CIs spanned approximately −600 to +400 µmol N m^{-2} h^{-1} (Table S5), reflecting high variability among replicate cores and the two control cores per site.

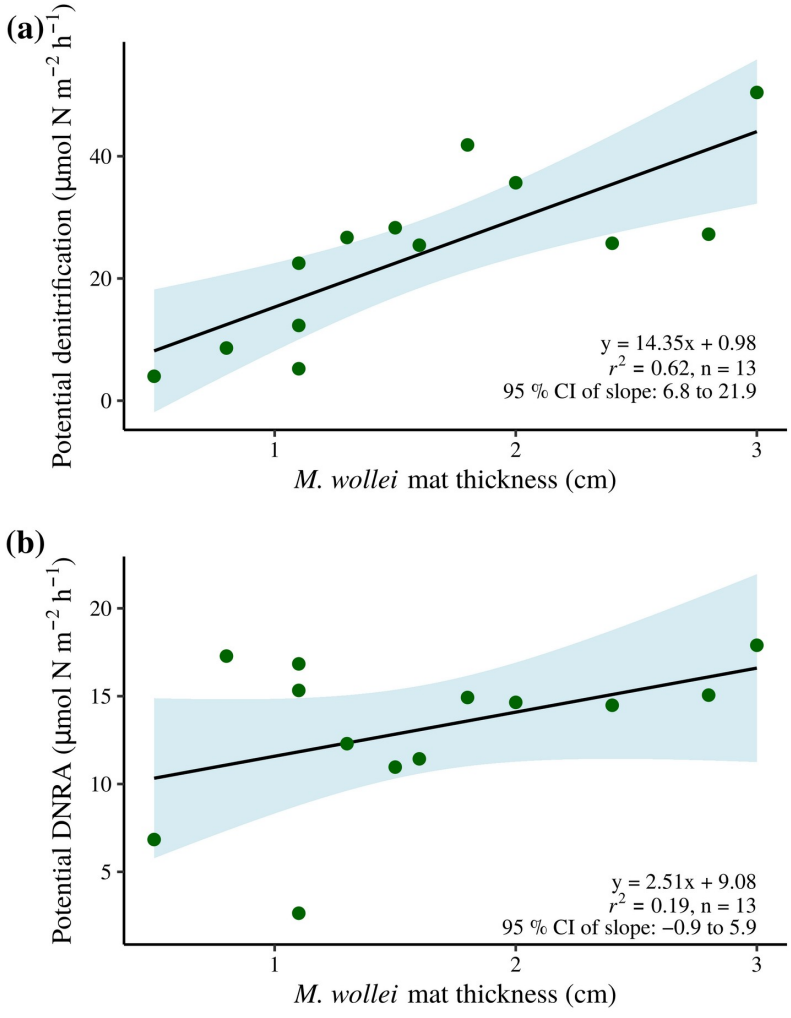
https://doi.org/10.5194/egusphere-2026-6811
Preprint. Discussion started: 11 November 2026
© Author(s) 2026. CC BY 4.0 License.



478

479 **Figure 4.** (a) Potential denitrification and (b) potential DNRA rates (measured using the OX/MIMS method
480 described in Yin et al. (2014)) in cores amended with $^{15}NO_3^-$ in the presence (green circles) and absence (orange
481 squares) of *M. wollei* benthic mats. Large symbols are means and error bars are standard deviations; small symbols
482 are individual sediment cores. The location sampled in each month is given below the month. March data are shown
483 for completeness but were excluded from the statistical analyses (Sect. 2.4). See Tables S4 and S5 for the statistical
484 analyses and Table S1 for the data.

https://doi.org/10.5194/egusphere-2026-6811
Preprint. Discussion started: 11 November 2026
© Author(s) 2026. CC BY 4.0 License.



485
486 **Figure 5.** (a) Potential denitrification and (b) potential DNRA rates (measured using the OX/MIMS method as in
487 Yin et al. (2014)) as a function of *M. wollei* mat thickness in mat cores. Lines are least-squares fits, and shaded areas
488 are 95 % confidence bands for the mean prediction (June–October cores, n = 13; the fits on the monthly means are
489 given in Sect. 3.4).

https://doi.org/10.5194/egusphere-2026-6811
Preprint. Discussion started: 11 November 2026
© Author(s) 2026. CC BY 4.0 License.

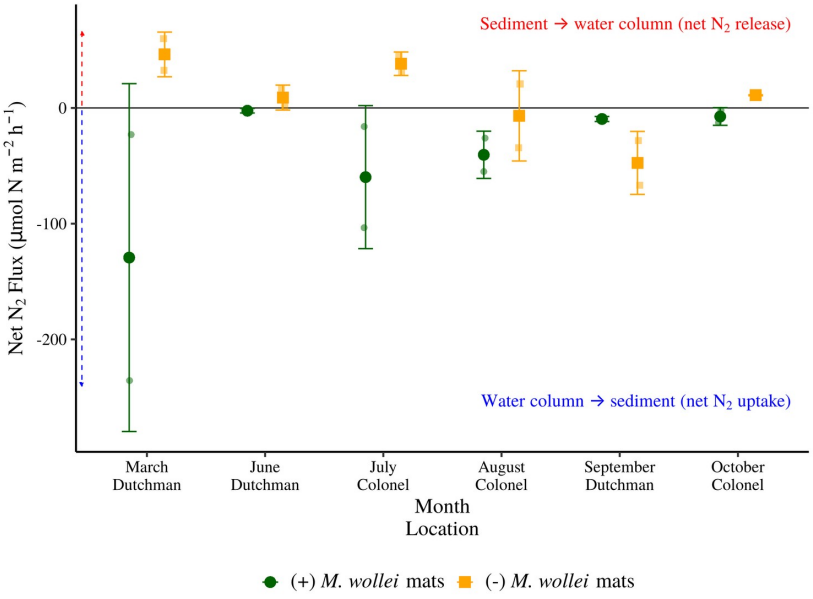


Figure 6. Net sediment–water N_2 flux in unamended control cores in the presence (green circles) and absence (orange squares) of *M. wollei* mats. Positive values indicate a net flux from the sediment to the water column (net N_2 release; denitrification exceeding N_2 fixation) and negative values a net flux from the water column into the sediment (net N_2 uptake; N_2 fixation exceeding denitrification). Large symbols are means and error bars are standard deviations; small symbols are individual cores. See Tables S4 and S5 for the statistical analyses and Table S1 for the data.

4 Discussion

Our paired comparison of sediments with and without *M. wollei* mats yielded five main results. 1) Mats raised porewater P and NO_3^- concentrations at the beginning of the season and porewater Fe concentrations during three out of the five months. However, porewater NH_4^+ concentrations beneath the mats did not exceed those found in bare sediment. 2) On average, potential denitrification rates did not differ between paired sites, although they did increase with increasing mat thickness. 3) Conversely, potential DNRA rates were higher at sites covered with benthic mats in four of the five months, although DNRA was not the dominant NO_3^- reduction pathway. 4) No anammox was detected. 5) Finally, the net N_2 flux in unamended mat cores was directed from the water column into the sediment, consistent with N_2 fixation exceeding denitrification. Below we discuss each result, place the rates in the context of other aquatic systems (Table 1), and consider the implications for internal nutrient loading (Sect. 4.6).

https://doi.org/10.5194/egusphere-2026-6811
Preprint. Discussion started: 11 November 2026
© Author(s) 2026. CC BY 4.0 License.

4.1 Mats mobilize sedimentary P and Fe

Benthic *M. wollei* mats created conditions that promoted the release of P and Fe within the mat horizon. Legacy P in the sediments sustains *M. wollei* growth in the shallow, oxygenated shoreline waters of Lake Wateree (Putnam et al., 2022), where soluble reactive P concentrations in the water column have generally been near the method detection limit of standard colorimetric methods (0.002 mg P L^{-1}) over the last four years (WaterWatch, 2025). Benthic mats can therefore rely on nutrients regenerated within the sediment (Vadeboncoeur et al., 2002; Stevenson et al., 2007). Porewater profiles similar to ours were observed beneath *M. wollei* in two Florida springs (Stevenson et al., 2007). The higher porewater P and Fe concentrations at mat sites are consistent with previous work at Lake Wateree showing that *M. wollei* growth depends on legacy sedimentary P (Putnam et al., 2022) and that most sediment P is bound to reducible Fe phases (Crandell, 2024), and most likely reflect enhanced deposition and remineralization of organic matter within the mat. These processes lower the redox potential in the underlying sediment and release Fe-bound P (Smolders et al., 2017; Ye et al., 2024). We did not measure sediment redox potential or pH, thus this mechanism is inferred from the co-variation of Fe, P, and O_2 concentrations rather than direct observations. For instance, the overlying water of mat cores contained about 50 µmol L^{-1} less O_2 than that of bare cores (Sect. 3.3), a difference that was already present at the start of the incubations.

However, P release is not a simple function of O_2, as organic and calcium-bound P can be remineralized under aerobic conditions, whereas aluminium-bound and non-reducible Fe(III) phases impede release (Hupfer and Lewandowski, 2008). At Lake Wateree, where sequential extractions have shown that more than 60 % of the sediment P is bound to reducible Fe phases (Crandell, 2024; Sect. 2.1), the elevated porewater Fe concentrations at mat sites in three of the five months, together with the elevated P concentrations in June and July, are consistent with reductive dissolution of Fe(III) phases as a release mechanism. Fe and P concentrations were both elevated in the same month only in June, however, and the mineral phases were not characterized here, so other release mechanisms cannot be excluded. Reactive P released in the anoxic part of the sediment may also reach the water column when bubbles of O_2, CO_2, or CH_4 generated within the mats lift mat material to the surface (Putnam et al., 2022).

https://doi.org/10.5194/egusphere-2026-6811
Preprint. Discussion started: 11 November 2026
© Author(s) 2026. CC BY 4.0 License.

4.2 Nitrogen cycling in the mat horizon and the fate of NH_4^+

Mats also altered porewater N early in the season: NO_3^- concentrations within the mat horizon were higher at mat sites in June and July, and NH_4^+ concentrations were lower at mat sites in June (Sect. 3.2). The early-season NO_3^- enrichment may reflect the remineralization of over-wintered mat biomass, which releases NH_4^+ that is rapidly nitrified in the oxic surface layer of the mat or assimilated by the growing mat. The lower NH_4^+ beneath the mats in June is consistent with such rapid conversion, and the thickness of the mats at Dutchman Creek decreased from 3.2 cm in March to 0.8 cm in June (Sect. 3.1), as expected if over-wintered biomass was decomposing. The disappearance of mat effects on porewater NO_3^- and P concentrations after July coincided with the presence of thin mats in August and peak period of mat biomass accumulation in the water column, during which the assimilation by the growing mat may have balanced remineralization. We however cannot separate remineralization from assimilation without measurements of mat biomass and turnover. Regardless of the balance between assimilation and remineralization, elevated P, Fe, and NO_3^- concentrations in the mat horizon early in the season, when the mats begin to grow, would favour rapid mat development (Sect. 4.1). The light treatment had no consistent effect on porewater nutrient concentrations after 24 h (only NO_2^- concentrations in August; Sect. 3.2), possibly because 24 h at 90–120 µmol photons m^{-2} s^{-1} was too short, or the irradiance too low, to shift the nutrient balance measurably at the depths sampled.

The mat sites were nevertheless a source of NH_4^+ to the overlying water in our incubation experiments. The NH_4^+ efflux estimated from its accumulation in mat cores during the incubations (Sect. 3.4) was 2–5 times the potential DNRA rate (scaled; Sect. 2.3.2) during the same month (Table S1). Potential DNRA rates could therefore account for about one fifth to two thirds of the NH_4^+ released by the mat-colonized sediments with any remaining portion originating from the mineralization of mat and sediment organic matter. NH_4^+ also accumulated in the bare cores, at rates (estimated from the change in concentration over the incubation; Sect. 3.4) that overlapped those of the mat cores. Therefore, results from the incubations do not show that mats raise the NH_4^+ efflux per unit area. However, NH_4^+ was consistently higher in the overlying water of the mat cores at the start of the incubations (Sect. 3.4), although part of this difference reflects the shallower overlying water of the mat cores (mean 13 vs. 20 cm; Sect. 2.1). The porewater NH_4^+ concentrations beneath the mats were never higher than in bare sediment

https://doi.org/10.5194/egusphere-2026-6811
Preprint. Discussion started: 11 November 2026
© Author(s) 2026. CC BY 4.0 License.

despite higher NH_4^+ production by DNRA. These results suggest that NH_4^+ is likely rapidly recycled within the mat, since cyanobacteria preferentially assimilate NH_4^+ relative to NO_3^- (Flores and Herrero, 2005). Furthermore, NH_4^+ generated at night or in anoxic microsites may be taken up by the mat during daytime.

4.3 Denitrification is the dominant N removal pathway and depends on mat thickness rather than on mat presence alone

Denitrification was the only N-removal pathway detected. $^{29}N_2$ production was below the method detection limit (approximately 1.1 µmol N m^{-2} h^{-1}; Sect. 2.3.2) in the $^{15}NH_4^+$-amended cores at all sites and during all months (Sect. 3.4). The $^{29}N_2$ signal in these cores includes any coupled nitrification–denitrification as well as anammox (Sect. 2.3.2), and rates below this limit would be a minor fraction of N_2 production except in June, when potential denitrification rates were lowest (4.6 and 1.9 µmol N m^{-2} h^{-1} with and without mats; Sect. 3.4; Table S1) and a rate at the method detection limit would have corresponded to 24–58 % of N_2 production. Anammox has been studied in comparatively few lakes, where it represents a variable fraction of total N_2 production: up to 10 % in the sediments of Missisquoi Bay, Lake Champlain (McCarthy et al., 2016), and 0 to 100 % (potential rates) in the bottom waters of Lake Erie, with the central basin acting as a hotspot (Lu et al., 2018). Anammox bacteria have also been detected in eutrophic lake sediments (Yoshinaga et al., 2011). The absence of detectable anammox in this study is consistent with the low porewater NO_2^- concentrations (< 0.02 mg N L^{-1}, i.e. < 1.5 µmol L^{-1}), since NO_2^- availability controls anammox communities in eutrophic lake sediments (Zhang et al., 2022), and with the C-rich sediments at both site types (Table S1), which favour heterotrophic NO_3^- reducers over anammox bacteria (Dalsgaard et al., 2005).

Mean potential denitrification rate did not differ between paired sites but increased strongly with mat thickness (Fig. 5a). These two results are consistent once mat thickness is taken into account. Where mat thickness was 1 cm or less (June and August), potential denitrification rates in mat cores were low and, in August, even below those in bare sediment. Conversely, where mat thickness was 1.5 cm or greater (i.e., in July, September, and October), potential denitrification rates exceeded that of bare sediment by a factor of 1.1–1.9 (Sect. 3.4). In June, a thin mat still supported more denitrification compared to bare sediment, which may reflect the presence of OC and NO_3^- released by over-wintered biomass (Sect. 4.2). The paired comparison of monthly means therefore suggests that mats affect denitrification in proportion to their thickness. With

https://doi.org/10.5194/egusphere-2026-6811
Preprint. Discussion started: 11 November 2026
© Author(s) 2026. CC BY 4.0 License.

five paired sampling events, the paired test could not detect a mean difference smaller than about 15 µmol N m^{-2} h^{-1}. However, the non-significant mean difference is not evidence that mats do not affect N removal. Mat presence is also confounded with site, since the paired sites lie 1–4 km apart and differ in grain size, porosity, and organic content (Table S1); the positive thickness relationship within each location (Sect. 3.4) and the agreement with earlier work at Lake Wateree (Putnam et al., 2022; Crandell, 2024) mitigate but do not remove this limitation.

Several mechanisms may explain why denitrification scales with mat thickness. Mat thickness is a proxy for the amount of mat material, including entrained litter, and therefore influences the supply of OC and the volume of anoxic microsites (Stal, 1995). Heterotrophic bacteria, including those attached to bloom-forming cyanobacteria (Yang et al., 2021), can reduce the NO_3^- supplied from the overlying water in those anoxic microsites. In our incubations the overlying water remained oxic (≥ 38 µmol O_2 L^{-1}; Sect. 3.3) and NO_3^--rich (Sect. 2.3.1), so the supply of NO_3^- to the mat was likely maintained, and under these conditions additional OC stimulates denitrification (Tiedje et al., 1983; Burgin and Hamilton, 2007). This contrasts with the accumulation of detritus from pelagic phytoplankton blooms on sediments in Lake Taihu, China, where O_2 depletion inhibited nitrification and uncoupled it from denitrification, reducing N removal (Zhu et al., 2020). Similarly, in tank experiments with Lake Taihu sediments, high phytoplankton biomass promoted DNRA but not N_2 production (Jiang et al., 2020b). Thick, living mats in oxic littoral water thus appear to enhance denitrification, whereas decaying pelagic biomass under hypoxic water suppresses it. The considerable variability in potential denitrification rates among replicate cores within a month, and the equally large within-month variability in sediment %C and %N (Table S1), suggest that the sediment microbial community and its OC supply are heterogeneous at the scale of individual cores, which could partially obscure the relationship between denitrification and mat thickness. Bulk organic content alone does not explain the pattern: the June mat sediments had the highest %C of the series (4.5 %; Table S1) but the lowest potential denitrification rates.

4.4 DNRA is higher beneath mats, but denitrification remains the major dissimilatory NO_3^- reduction pathway

DNRA accounted for 39 % of total dissimilatory NO_3^- reduction in mat cores and 29 % in bare sediment cores. These shares are above the 3–22 % reported for other lake sediments (Nizzoli et al., 2010; Jiang et al., 2020a), where DNRA may not even be a consistent NH_4^+ regeneration

https://doi.org/10.5194/egusphere-2026-6811
Preprint. Discussion started: 11 November 2026
© Author(s) 2026. CC BY 4.0 License.

pathway (McCarthy et al., 2016). Yet, the fraction of DNRA relative to total dissimilatory NO_3^- reduction calculated in this study is within or close to the ranges reported for organic-rich, reducing lake sediments (31–50 %; Souza et al., 2012; Robertson and Thamdrup, 2017; Cojean et al., 2020) and reducing riparian sediments (10–79 %; Rahman et al., 2024). Furthermore, the potential DNRA rates fall within the range reported for lakes and wetlands (Table 1).

Table 1. Sediment denitrification, DNRA, and N_2 fixation in this study compared with published values from lakes, reservoirs, and other freshwater and estuarine sediments. Units are given with each value; areal rates are in µmol N m^{-2} h^{-1}. Slurry-based (volumetric) potential rates are not directly comparable with areal rates and are listed with their original units. n.m. = not measured; n.r. = not reported in a comparable format.

System	Method	Denitrification	DNRA	DNRA (% of NO_3^- reduction)	N_2 fixation / net N_2 flux	Reference
Lake Wateree, SC, USA – littoral sediment with *M. wollei* mats	Intact cores, $^{15}NO_3^-$ IPT + OX/MIMS (DNRA as $^{15}NH_4^+$ production); N_2:Ar in unamended cores	24.2 ± 13.9 µmol N m^{-2} h^{-1} (monthly means 4.6–34.5 µmol N m^{-2} h^{-1})	13.1 ± 4.4 µmol N m^{-2} h^{-1} (monthly means 4.7–17.1 µmol N m^{-2} h^{-1})	39 %	Net N_2 flux −23.9 ± 32.2 µmol N m^{-2} h^{-1} (into the sediment in all months)	This study
Lake Wateree – bare littoral sediment	As above	19.3 ± 12.2 µmol N m^{-2} h^{-1} (monthly means 1.9–30.9 µmol N m^{-2} h^{-1})	5.8 ± 3.3 µmol N m^{-2} h^{-1} (monthly means 2.4–9.1 µmol N m^{-2} h^{-1})	29 %	Net N_2 flux +0.8 ± 34.0 µmol N m^{-2} h^{-1}	This study
Ca' Stanga (mesotrophic) and Lago Verde (hypertrophic), Italy – hypolimnetic sediment	Intact cores, ^{15}N IPT	29–171 µmol N m^{-2} h^{-1} (0.7–4.1 mmol N m^{-2} d^{-1})	2.9–5.0 µmol N m^{-2} h^{-1} (0.07–0.12 mmol N m^{-2} d^{-1})	3–15 %	n.m.	Nizzoli et al. (2010)
Three small reservoirs, Arkansas, USA	In situ N_2 accumulation + intact cores	99–168 µmol N m^{-2} h^{-1} (hypolimnion)	n.m.	–	Net N_2 fixation during summer stratification	Grantz et al. (2012)
Missisquoi Bay, Lake Champlain, USA/Canada	Continuous-flow intact cores, ^{15}N + N_2:Ar	Net N_2 flux (not potential denitrification) 159 ± 53 µmol N m^{-2} h^{-1} at the river mouth and 1 ± 28 µmol N m^{-2} h^{-1} in the central basin	Potential DNRA 0–29 µmol N m^{-2} h^{-1}; above zero on 6 of 23 sampling dates; not a consistent NH_4^+ regeneration pathway	About one third (≈ 33 %) at the river mouth when detected	N_2 fixation throughout the ice-free season, compensating 25–30 % of N losses; anammox ≤ 10 % of N_2 production	McCarthy et al. (2016)

https://doi.org/10.5194/egusphere-2026-6811
Preprint. Discussion started: 11 November 2026
© Author(s) 2026. CC BY 4.0 License.

System	Method	Denitrification	DNRA	DNRA (% of NO_3^- reduction)	N_2 fixation / net N_2 flux	Reference
Lake Taihu, China – shallow hypereutrophic	Intact cores (field and tank experiment), net N_2 flux	Experiment: 66 µmol N m^{-2} h^{-1} without and 836 µmol N m^{-2} h^{-1} with added algal biomass, 570 and 174 µmol N m^{-2} h^{-1} under low and high algal accumulation; field: 187–226 µmol N m^{-2} h^{-1} in spring, < 10 µmol N m^{-2} h^{-1} in summer; lake-scale estimates of 167 and 77 µmol N m^{-2} h^{-1} when algal biomass accumulates over 20 % and 10 % of the lake area	n.m.	–	n.m.	Zhu et al. (2020)
27 lakes, Eastern Plain, China	^{15}N slurry potential rates	Dominant (n.r.)	n.r.	4–22 %	n.m.	Jiang et al. (2020a)
Lake Taihu – algal accumulation experiment	^{15}N slurry incubations (potential rates, µmol N kg^{-1} h^{-1}) of sediment from tank experiments with added algal biomass	Not stimulated by algal biomass	Stimulated by algal biomass; controlled by dissolved organic carbon (DOC)	Increases with DOC:NO_3^-	n.m.	Jiang et al. (2020b)
Lake Lugano, Switzerland	Anoxic ^{15}N slurries	53–85 nmol N g^{-1} wet sediment d^{-1}	38–44 nmol N g^{-1} wet sediment d^{-1}	31–46 %	n.m. (anammox ≈ 0.01 nmol N g^{-1} d^{-1}, < 1 % of N removal)	Cojean et al. (2020)
Lake Almind, Denmark	^{15}N slurries with Fe^{2+} amendment	4.7–4.8 µmol N L^{-1} d^{-1} (unamended slurries)	2.5–3.7 µmol N L^{-1} d^{-1} (unamended); stimulated by Fe^{2+}	35–47 % (unamended; from the rates in their Table 2)	n.m. (anammox negligible)	Robertson and Thamdrup (2017)
Floodplain lake, Pantanal, Brazil	Intact cores, IPT	7–69 µmol N m^{-2} h^{-1} (3.4–34.5 µmol N_2 m^{-2} h^{-1})	Not measured; estimated as the $^{15}NO_3^-$ not recovered as N_2	≈ 50 % (by difference)	n.m. (anammox negligible)	Souza et al. (2012)
Lake Waco Wetland, Texas, USA – created freshwater wetland	Continuous-flow intact cores, ^{15}N + MIMS	54–278 µmol N m^{-2} h^{-1}	1.3–33 µmol N m^{-2} h^{-1} (summer only)	5 % on average (up to 36 % at one site)	N_2 fixation 0–426 µmol N m^{-2} h^{-1}; net N_2 flux +184 to −270 µmol N m^{-2} h^{-1}	Scott et al. (2008)
Old Woman Creek, Lake Erie coastal wetland, USA	Continuous-flow intact cores, ^{15}N + MIMS	Net N_2 efflux at all times	Present at the wetland sites, not at the lake site	Denitrification:DNRA > 17 (2 at one site)	Net N_2 efflux (denitrification > fixation)	McCarthy et al. (2007)
Four Texas estuaries, USA	Continuous-flow intact cores, ^{15}N + MIMS	0–90 µmol N m^{-2} h^{-1}	0–80 µmol N m^{-2} h^{-1} (potential, as $^{15}NH_4^+$ accumulation); NH_4^+ efflux up to about 300 µmol N m^{-2} h^{-1}	n.r.	N_2 fixation 0–97 µmol N m^{-2} h^{-1}	Gardner et al. (2006)

https://doi.org/10.5194/egusphere-2026-6811
Preprint. Discussion started: 11 November 2026
© Author(s) 2026. CC BY 4.0 License.

System	Method	Denitrification	DNRA	DNRA (% of NO_3^- reduction)	N_2 fixation / net N_2 flux	Reference
Constructed stormwater wetlands, Melbourne, Australia	^{15}N slurries	2.0–8.0 (high OC:NO_3^-) to 13.5–68 (low OC:NO_3^-) µmol N L^{-1} h^{-1}	0.2–1.2 (high OC:NO_3^-) to 1.7–18 (low OC:NO_3^-) µmol N L^{-1} h^{-1}; 1.5–3.5× higher with Fe^{2+}	4–30 % (higher with Fe^{2+})	n.m. (anammox < 0.05 %)	Rahman et al. (2019)
Riparian sediments at relict milldams, USA	^{15}N slurries	n.r.	5.2–37.6 µg N L^{-1} h^{-1}	10–79 %	n.m.	Rahman et al. (2024)

Values from this study are means ± SD of individual cores from June to October 2023 (n = 13 with mats and 12 without mats for denitrification and DNRA; n = 10 and 10 for the net N_2 flux); monthly means are given in Table S1. Literature values were taken from the cited papers' abstracts or tables as indicated; where a paper reported only a qualitative result, this is stated in words. DNRA from this study is scaled to the whole NO_3^- pool by dividing by the ^{15}N fraction of the overlying-water NO_3^- (Sect. 2.3.2); all rates from this study were measured at 16–17 °C.

DNRA is favoured over denitrification when electron donors (OC, Fe(II)) are in excess relative to NO_3^- (Tiedje, 1988; Hardison et al., 2015; Rahman et al., 2019). Under the oxic, NO_3^--rich conditions of our incubations (Sect. 4.3), denitrification is expected to dominate. Three properties of the mats can nevertheless explain why potential DNRA rates were 2.3 times higher in their presence. First, mats supply labile OC, whose composition influences the end products of NO_3^- respiration (Carlson et al., 2020). Second, they raise porewater Fe concentrations (measured as total dissolved Fe, which in anoxic porewater is mostly Fe(II)). Fe(II) is an electron donor for chemolithotrophic DNRA (Robertson and Thamdrup, 2017; Yuan et al., 2022), and Fe(II) addition stimulates DNRA at the expense of denitrification (Robertson and Thamdrup, 2017; Rahman et al., 2019). Third, assimilation by mats may deplete NO_3^- locally, since cyanobacteria assimilate NO_3^- when NH_4^+ is scarce (Flores and Herrero, 2005). Yet porewater NO_3^- concentrations in the mat horizon were not lower at the mat sites (Sect. 3.2), thus this third mechanism is not supported by our porewater nutrient concentration data. The correlations between potential DNRA rates and initial nutrient concentrations are consistent with this model of substrate control: potential DNRA rates were positively correlated with NH_4^+ concentrations in the overlying water and negatively, though not significantly, with NO_3^- and NO_2^- concentrations, whereas potential denitrification rates were correlated with none of these variables (Table S6). The scaling of the DNRA rates by the ^{15}N fraction (Sect. 2.3.2), which depends on the ambient NO_3^- concentration, also weakens any negative relationship with NO_3^-. Potential DNRA rates also tended to increase with mat thickness, but much more weakly than denitrification (Fig. 5b; Sect. 3.4). DNRA thus appears to respond to the supply of electron

https://doi.org/10.5194/egusphere-2026-6811
Preprint. Discussion started: 11 November 2026
© Author(s) 2026. CC BY 4.0 License.

donors (OC, Fe(II)) at the mat–sediment interface, which is altered in the presence of a mat, whereas denitrification responds to the volume of mat in which NO_3^- can be reduced.

The scaled potential DNRA rates assume that the ^{15}N fraction of the NO_3^- reduced in the sediment equalled that of the overlying water (Sect. 2.3.2); because the same assumption applies to both site types, it is unlikely to bias the comparison between mat and bare cores. Because the rates are based on the $^{15}NH_4^+$ recovered in the overlying water, they may underestimate the production (Sect. 2.3.2), particularly for the mat cores. The potential rates were also measured under conditions that differ from those in situ: the tracer raised the overlying-water NO_3^- concentration by 50–115 %, which favours denitrification over DNRA, and the incubation temperature (16–17 °C) was well below summer in situ temperatures (> 30 °C).

We emphasize that DNRA recycles N but does not necessarily retain it in the lake. The NH_4^+ it produces can be exported to the water column, assimilated, or nitrified and subsequently denitrified (Sect. 4.2), and determining whether the mats increase long-term N retention would require long-term ^{15}N tracing at the ecosystem scale. Although DNRA was not the dominant dissimilatory NO_3^- reduction pathway, it nevertheless increases the residence time of bioavailable N in the littoral zone and supplies NH_4^+, which is an internal N source for blooms (Hoffman et al., 2022), at the sediment–water interface.

4.5 Net N_2 flux into the sediment suggests N_2 fixation beneath mats

In all ten mat cores, the net N_2 flux was directed from the water column into the sediment, whereas in bare cores the direction of the flux reversed over the months, overall averaging out to a value close to zero (Sect. 3.4). Neither the difference between site types nor the mean flux of the mat cores differed significantly from zero, and the net N_2 fluxes rest on only two control cores per site. Yet, the consistent direction of the flux indicates that N_2 fixation likely exceeded denitrification beneath the mats during the incubations. To our knowledge, these are the first areal net N_2 flux measurements beneath *M. wollei* mats. They are consistent with acetylene-reduction evidence that *M. wollei* mats and cultures fix N_2, with activity suppressed by O_2 and enhanced by light–dark cycling (Phlips et al., 1992), and with nitrogenase activity measured in freshwater benthic cyanobacterial communities that included *Lyngbya* (Lam et al., 1979). O_2 production by the mats under the room light of the incubations, evident in July (Sect. 3.3), can promote bubble formation that strips N_2 from the porewater and biases N_2:Ar-derived fluxes

https://doi.org/10.5194/egusphere-2026-6811
Preprint. Discussion started: 11 November 2026
© Author(s) 2026. CC BY 4.0 License.

towards an apparent flux into the sediment (Eyre et al., 2002); the flux was also directed into the sediment in the four months in which O_2 declined, so the direction of the net flux is unlikely to be an artefact.

Although elevated DIN can depress N_2 fixation (Knapp, 2012) and denitrification exceeded N_2 fixation in, for example, a Lake Erie coastal wetland (McCarthy et al., 2007), net N_2 fixation has been measured in coastal marine (Fulweiler et al., 2007), estuarine, wetland, reservoir, and lake sediments at rates that bracket ours (Table 1). Several properties of the mat environment favour N_2 fixation despite the high ambient DIN. In the sediments of a eutrophic, bloom-affected bay of Lake Taihu, N_2 fixation occurred and was controlled primarily by porewater sulfide (Tian et al., 2021). The same supply of labile extracellular OC and anoxic microsites that supports denitrification (Sect. 4.3) fuels the energetically expensive nitrogenase reaction (Howarth et al., 1988; Fulweiler et al., 2013) and hosts heterotrophic N_2-fixing bacteria (diazotrophs), including sulfate-reducing bacteria (Bertics et al., 2013). The close association of these heterotrophic diazotrophs with the cyanobacteria promotes N_2 fixation within the mat consortium (Paerl, 1977; Paerl et al., 1996). Nitrogenase requires Fe (Hoffman et al., 2014) and N_2 fixation requires P (Howarth et al., 1988; Lu et al., 2019). The elevated porewater Fe and P at the mat sites (Sect. 4.1) therefore also favour N_2 fixation by *M. wollei* and its associated heterotrophs.

4.6 Implications for internal nutrient loading and lake management

Benthic producers are often overlooked in lake nutrient budgets (Vadeboncoeur et al., 2002) even though benthic algal proliferations are increasing (Hampton et al., 2024). Our results (Sects. 4.1–4.5) indicate that *M. wollei* mats are hotspots of N turnover rather than solely N sources. The net effect of mats on a whole-lake N budget will depend on the areal extent and thickness of the mats, on the fate of the NH_4^+ they export, and on hydraulic export and burial, none of which we quantified. Scaling our core-based rates to the lake would require in situ measurements across the mat zone (Sect. 2.1; Fig. S2). We expect similar effects wherever dense filamentous mats, with their steep internal gradients and three-dimensional consortium, colonize organic-rich littoral sediments. In contrast, non-mat-forming benthic cyanobacteria such as *Gloeotrichia*, which translocate sediment nutrients into the water column when they recruit (Cottingham et al., 2015), would not be expected to have the same effects.

https://doi.org/10.5194/egusphere-2026-6811
Preprint. Discussion started: 11 November 2026
© Author(s) 2026. CC BY 4.0 License.

Our results have three implications for management. First, because *M. wollei* mats release legacy P and recycle N, they may sustain eutrophication and cyanobacterial blooms even when external loads are reduced (Wurtsbaugh et al., 2019), as internal N sources such as N_2 fixation can sustain non-N_2-fixing blooms (Beversdorf et al., 2013). Second, if the relationship between mat thickness and denitrification holds in situ, the physical removal of thick mats would remove a source of P, NH_4^+, and newly fixed N but also sediment with a high capacity to reduce NO_3^-; the net effect on the N budget cannot be predicted from our data. Third, the largest mat effects on porewater P and NO_3^- occurred in June and July, when the mats begin to grow; whether early-season porewater is the most sensitive indicator of mat-driven internal loading should be tested by repeated sampling at the same sites. Priorities for future work on lakes affected by benthic cyanobacterial mats are to validate the thickness–denitrification relationship with in situ rates across seasons and across lakes with different sediment types; quantify P mobilization rates and the genes and transcripts of denitrifiers, DNRA bacteria, and diazotrophs (*nirS*, *nirK*, *nrfA*, *nifH*); trace the fate of NH_4^+ and ^{15}N within the mat; and measure $^{30}N_2$ uptake directly, which would resolve the contribution of *M. wollei* itself relative to its associated heterotrophs.

5 Conclusions

This study shows that benthic *M. wollei* mats can be an important source of internal nutrient recycling that complicates the management of eutrophic lakes. Benthic *M. wollei* mats in Lake Wateree increased porewater P and NO_3^- concentrations early in the growing season and porewater Fe concentrations in three of the five months. Potential denitrification rates did not differ on average between sediments with and without mats, but they increased with mat thickness. Thick mats enhanced N removal, whereas thin mats did not consistently raise it above that of bare sediment. Anammox was not detected. Potential DNRA rates were 2.3 times higher in the presence of mats and accounted for 39 % of total NO_3^- reduction beneath them. Yet, denitrification remained the larger dissimilatory NO_3^- reduction pathway in both sediment types. In unamended mat cores, the net N_2 flux was directed from the water column into the sediment during every month, indicating that N_2 fixation, in the mats or in the overlying water of the cores, likely exceeded denitrification, and the water overlying mat-colonized sediments was consistently enriched in NH_4^+. Overall, *M. wollei* mats act as hotspots of N turnover: where thick,

https://doi.org/10.5194/egusphere-2026-6811
Preprint. Discussion started: 11 November 2026
© Author(s) 2026. CC BY 4.0 License.

they remove N through denitrification, but they also regenerate NH_4^+, likely fix N_2, and mobilize legacy P in the mat horizon.

Code and data availability

All data, the rate calculations, and the R scripts used for the statistical analyses and figures are available in the Open Science Framework repository at https://doi.org/10.17605/OSF.IO/D98XZ (Venkatachari et al., 2025).

Supplement

The supplement related to this article is available online.

Author contributions

AV performed all fieldwork, laboratory experiments, and sample and data analyses and wrote the first draft of the manuscript (investigation, formal analysis, writing – original draft). AB secured funding, assisted with the laboratory experiments, data analysis, and rate calculations, and contributed to writing (funding acquisition, supervision, formal analysis, investigation, writing – review and editing). KLC secured funding, guided the statistical analyses and reviewed and edited the manuscript (funding acquisition, supervision, formal analysis, writing – review and editing).

Competing interests

The contact author has declared that none of the authors has any competing interests.

Acknowledgements

We are grateful to Dalton John Hite for his help with sample collection in the field and with the ^{15}N-labelled whole-core incubations in the laboratory, and to Darcy Perin and Clare Matta for training students for the first set of field and incubation experiments. We thank the residents of Lake Wateree for providing access to their docks for sample collection, and we thank Claudia Benitez-Nelson, James Pinckney, Matthew Baumann, and Xuefeng (Nick) Peng, the members of AV's dissertation committee, for their comments on an earlier version of this work. Grammarly was used for grammatical corrections during the preparation of the manuscript, and ChatGPT

https://doi.org/10.5194/egusphere-2026-6811
Preprint. Discussion started: 11 November 2026
© Author(s) 2026. CC BY 4.0 License.

was used to assist with plotting code in RStudio; no text or scientific content was generated by these tools.

Financial support

This research has been supported by the National Science Foundation (grant no. 1923004) and by a recurring annual award from the Lake Wateree Association to AB in support of the WaterWatch water quality monitoring programme. AV was also partially supported by the Hank McKellar Fellowship of the Society of Lake Management Professionals and by the South Carolina Aquatic Plant Management Society.

References

Bertics, V. J., Löscher, C. R., Salonen, I., Dale, A. W., Gier, J., Schmitz, R. A., and Treude, T.: Occurrence of benthic microbial nitrogen fixation coupled to sulfate reduction in the seasonally hypoxic Eckernförde Bay, Baltic Sea, Biogeosciences, 10, 1243–1258, https://doi.org/10.5194/bg-10-1243-2013, 2013.

Beversdorf, L. J., Miller, T. R., and McMahon, K. D.: The role of nitrogen fixation in cyanobacterial bloom toxicity in a temperate, eutrophic lake, PLoS ONE, 8, e56103, https://doi.org/10.1371/journal.pone.0056103, 2013.

Bonaglia, S., Deutsch, B., Bartoli, M., Marchant, H. K., and Brüchert, V.: Seasonal oxygen, nitrogen and phosphorus benthic cycling along an impacted Baltic Sea estuary: regulation and spatial patterns, Biogeochemistry, 119, 139–160, https://doi.org/10.1007/s10533-014-9953-6, 2014.

Brunet, R. C. and Garcia-Gil, L. J.: Sulfide-induced dissimilatory nitrate reduction to ammonia in anaerobic freshwater sediments, FEMS Microbiol. Ecol., 21, 131–138, https://doi.org/10.1111/j.1574-6941.1996.tb00340.x, 1996.

Burgin, A. J. and Hamilton, S. K.: Have we overemphasized the role of denitrification in aquatic ecosystems? A review of nitrate removal pathways, Front. Ecol. Environ., 5, 89–96, https://doi.org/10.1890/1540-9295(2007)5[89:HWOTRO]2.0.CO;2, 2007.

Carlson, H. K., Lui, L. M., Price, M. N., Kazakov, A. E., Carr, A. V., Kuehl, J. V., Owens, T. K., Nielsen, T., Arkin, A. P., and Deutschbauer, A. M.: Selective carbon sources influence the end products of microbial nitrate respiration, ISME J., 14, 2034–2045, https://doi.org/10.1038/s41396-020-0666-7, 2020.

Cojean, A. N. Y., Lehmann, M. F., Robertson, E. K., Thamdrup, B., and Zopfi, J.: Controls of H_2S, Fe^{2+}, and Mn^{2+} on microbial NO_3^--reducing processes in sediments of an eutrophic lake, Front. Microbiol., 11, 1158, https://doi.org/10.3389/fmicb.2020.01158, 2020.

https://doi.org/10.5194/egusphere-2026-6811
Preprint. Discussion started: 11 November 2026
© Author(s) 2026. CC BY 4.0 License.



Cottingham, K. L., Ewing, H. A., Greer, M. L., Carey, C. C., and Weathers, K. C.: Cyanobacteria as biological drivers of lake nitrogen and phosphorus cycling, Ecosphere, 6, 1–19, https://doi.org/10.1890/ES14-00174.1, 2015.

Crandell, C. A.: Detection and analysis of solid-phase nutrients in complex benthic cyanobacterium communities, PhD thesis, University of South Carolina, Columbia, SC, USA, https://scholarcommons.sc.edu/etd/7699 (last access: 27 September 2026), 2024.

Dalsgaard, T., Thamdrup, B., and Canfield, D. E.: Anaerobic ammonium oxidation (anammox) in the marine environment, Res. Microbiol., 156, 457–464, https://doi.org/10.1016/j.resmic.2005.01.011, 2005.

Dodds, W. K., Bouska, W. W., Eitzmann, J. L., Pilger, T. J., Pitts, K. L., Riley, A. J., Schloesser, J. T., and Thornbrugh, D. J.: Eutrophication of U.S. freshwaters: analysis of potential economic damages, Environ. Sci. Technol., 43, 12–19, https://doi.org/10.1021/es801217q, 2009.

Dong, L. F., Smith, C. J., Papaspyrou, S., Stott, A., Osborn, A. M., and Nedwell, D. B.: Changes in benthic denitrification, nitrate ammonification, and anammox process rates and nitrate and nitrite reductase gene abundances along an estuarine nutrient gradient (the Colne estuary, United Kingdom), Appl. Environ. Microbiol., 75, 3171–3179, https://doi.org/10.1128/AEM.02511-08, 2009.

Eyre, B. D., Rysgaard, S., Dalsgaard, T., and Christensen, P. B.: Comparison of isotope pairing and N_2:Ar methods for measuring sediment denitrification – assumptions, modifications, and implications, Estuaries, 25, 1077–1087, https://doi.org/10.1007/BF02692205, 2002.

Flores, E. and Herrero, A.: Nitrogen assimilation and nitrogen control in cyanobacteria, Biochem. Soc. Trans., 33, 164–167, https://doi.org/10.1042/BST0330164, 2005.

Fulweiler, R. W. and Nixon, S. W.: Net sediment N_2 fluxes in a southern New England estuary: variations in space and time, Biogeochemistry, 111, 111–124, https://doi.org/10.1007/s10533-011-9660-5, 2012.

Fulweiler, R. W., Nixon, S. W., Buckley, B. A., and Granger, S. L.: Reversal of the net dinitrogen gas flux in coastal marine sediments, Nature, 448, 180–182, https://doi.org/10.1038/nature05963, 2007.

Fulweiler, R. W., Brown, S. M., Nixon, S. W., and Jenkins, B. D.: Evidence and a conceptual model for the co-occurrence of nitrogen fixation and denitrification in heterotrophic marine sediments, Mar. Ecol. Prog. Ser., 482, 57–68, https://doi.org/10.3354/meps10240, 2013.

Gardner, W. S., McCarthy, M. J., An, S., Sobolev, D., Sell, K. S., and Brock, D.: Nitrogen fixation and dissimilatory nitrate reduction to ammonium (DNRA) support nitrogen dynamics in Texas estuaries, Limnol. Oceanogr., 51, 558–568, https://doi.org/10.4319/lo.2006.51.1_part_2.0558, 2006.

https://doi.org/10.5194/egusphere-2026-6811
Preprint. Discussion started: 11 November 2026
© Author(s) 2026. CC BY 4.0 License.



849 Grantz, E. M., Kogo, A., and Scott, J. T.: Partitioning whole-lake denitrification using in situ
850 dinitrogen gas accumulation and intact sediment core experiments, Limnol. Oceanogr., 57,
851 925–935, https://doi.org/10.4319/lo.2012.57.4.0925, 2012.

852 Grasshoff, K., Kremling, K., and Ehrhardt, M. (Eds.): Methods of Seawater Analysis, 3rd,
853 completely revised and extended edn., Wiley-VCH, Weinheim, Germany,
854 https://doi.org/10.1002/9783527613984, 1999.

855 Gruber, N. and Galloway, J. N.: An Earth-system perspective of the global nitrogen cycle,
856 Nature, 451, 293–296, https://doi.org/10.1038/nature06592, 2008.

857 Hamme, R. C. and Emerson, S. R.: The solubility of neon, nitrogen and argon in distilled water
858 and seawater, Deep-Sea Res. Pt. I, 51, 1517–1528,
859 https://doi.org/10.1016/j.dsr.2004.06.009, 2004.

860 Hampton, S. E., Baron, J. S., Ladwig, R., McClure, R. P., Meyer, M. F., Oleksy, I. A., and
861 Shampain, A.: Warming-induced changes in benthic redox as a potential driver of
862 increasing benthic algal blooms in high-elevation lakes, Limnol. Oceanogr. Lett., 9, 1–6,
863 https://doi.org/10.1002/lol2.10357, 2024.

864 Hardison, A. K., Algar, C. K., Giblin, A. E., and Rich, J. J.: Influence of organic carbon and
865 nitrate loading on partitioning between dissimilatory nitrate reduction to ammonium
866 (DNRA) and N_2 production, Geochim. Cosmochim. Ac., 164, 146–160,
867 https://doi.org/10.1016/j.gca.2015.04.049, 2015.

868 Hoffman, B. M., Lukoyanov, D., Yang, Z.-Y., Dean, D. R., and Seefeldt, L. C.: Mechanism of
869 nitrogen fixation by nitrogenase: the next stage, Chem. Rev., 114, 4041–4062,
870 https://doi.org/10.1021/cr400641x, 2014.

871 Hoffman, D. K., McCarthy, M. J., Boedecker, A. R., Myers, J. A., and Newell, S. E.: The role of
872 internal nitrogen loading in supporting non-N-fixing harmful cyanobacterial blooms in the
873 water column of a large eutrophic lake, Limnol. Oceanogr., 67, 2028–2041,
874 https://doi.org/10.1002/lno.12185, 2022.

875 Holm, S.: A simple sequentially rejective multiple test procedure, Scand. J. Stat., 6, 65–70, 1979.

876 Howarth, R. W., Marino, R., and Cole, J. J.: Nitrogen fixation in freshwater, estuarine, and
877 marine ecosystems. 2. Biogeochemical controls, Limnol. Oceanogr., 33, 688–701,
878 https://doi.org/10.4319/lo.1988.33.4part2.0688, 1988.

879 Hupfer, M. and Lewandowski, J.: Oxygen controls the phosphorus release from lake sediments –
880 a long-lasting paradigm in limnology, Int. Rev. Hydrobiol., 93, 415–432,
881 https://doi.org/10.1002/iroh.200711054, 2008.

882 Jensen, H. S. and Andersen, F. Ø.: Importance of temperature, nitrate, and pH for phosphate
883 release from aerobic sediments of four shallow, eutrophic lakes, Limnol. Oceanogr., 37,
884 577–589, https://doi.org/10.4319/lo.1992.37.3.0577, 1992.

https://doi.org/10.5194/egusphere-2026-6811
Preprint. Discussion started: 11 November 2026
© Author(s) 2026. CC BY 4.0 License.



885 Jiang, X., Gao, G., Zhang, L., Tang, X., Shao, K., and Hu, Y.: Denitrification and dissimilatory
886 nitrate reduction to ammonium in freshwater lakes of the Eastern Plain, China: influences
887 of organic carbon and algal bloom, Sci. Total Environ., 710, 136303,
888 https://doi.org/10.1016/j.scitotenv.2019.136303, 2020a.

889 Jiang, X., Gao, G., Zhang, L., Tang, X., Shao, K., Hu, Y., and Cai, J.: Role of algal
890 accumulations on the partitioning between N_2 production and dissimilatory nitrate
891 reduction to ammonium in eutrophic lakes, Water Res., 183, 116075,
892 https://doi.org/10.1016/j.watres.2020.116075, 2020b.

893 Kana, T. M., Darkangelo, C., Hunt, M. D., Oldham, J. B., Bennett, G. E., and Cornwell, J. C.:
894 Membrane inlet mass spectrometer for rapid high-precision determination of N_2, O_2, and
895 Ar in environmental water samples, Anal. Chem., 66, 4166–4170,
896 https://doi.org/10.1021/ac00095a009, 1994.

897 Knapp, A. N.: The sensitivity of marine N_2 fixation to dissolved inorganic nitrogen, Front.
898 Microbiol., 3, 374, https://doi.org/10.3389/fmicb.2012.00374, 2012.

899 Lam, C. W. Y., Vincent, W. F., and Silvester, W. B.: Nitrogenase activity and estimates of
900 nitrogen fixation by freshwater benthic blue-green algae, New Zeal. J. Mar. Fresh., 13,
901 187–192, https://doi.org/10.1080/00288330.1979.9515793, 1979.

902 Lévesque, D., Cattaneo, A., Hudon, C., and Gagnon, P.: Predicting the risk of proliferation of the
903 benthic cyanobacterium *Lyngbya wollei* in the St. Lawrence River, Can. J. Fish. Aquat.
904 Sci., 69, 1585–1595, https://doi.org/10.1139/f2012-087, 2012.

905 Lu, J., Zhu, B., Struewing, I., Xu, N., and Duan, S.: Nitrogen–phosphorus-associated metabolic
906 activities during the development of a cyanobacterial bloom revealed by
907 metatranscriptomics, Sci. Rep., 9, 2480, https://doi.org/10.1038/s41598-019-38481-2,
908 2019.

909 Lu, X., Bade, D. L., Leff, L. G., and Mou, X.: The relative importance of anammox and
910 denitrification to total N_2 production in Lake Erie, J. Great Lakes Res., 44, 428–435,
911 https://doi.org/10.1016/j.jglr.2018.03.008, 2018.

912 McCarthy, M. J., Gardner, W. S., Lavrentyev, P. J., Moats, K. M., Jochem, F. J., and Klarer, D.
913 M.: Effects of hydrological flow regime on sediment-water interface and water column
914 nitrogen dynamics in a Great Lakes coastal wetland (Old Woman Creek, Lake Erie), J.
915 Great Lakes Res., 33, 219–231, https://doi.org/10.3394/0380-
916 1330(2007)33[219:EOHFRO]2.0.CO;2, 2007.

917 McCarthy, M. J., Gardner, W. S., Lehmann, M. F., Guindon, A., and Bird, D. F.: Benthic
918 nitrogen regeneration, fixation, and denitrification in a temperate, eutrophic lake: effects on
919 the nitrogen budget and cyanobacteria blooms, Limnol. Oceanogr., 61, 1406–1423,
920 https://doi.org/10.1002/lno.10306, 2016.

https://doi.org/10.5194/egusphere-2026-6811
Preprint. Discussion started: 11 November 2026
© Author(s) 2026. CC BY 4.0 License.

McGregor, G. B. and Sendall, B. C.: Phylogeny and toxicology of *Lyngbya wollei* (Cyanobacteria, Oscillatoriales) from north-eastern Australia, with a description of *Microseira* gen. nov., J. Phycol., 51, 109–119, https://doi.org/10.1111/jpy.12256, 2015.

Meyers, P. A. and Teranes, J. L.: Sediment organic matter, in: Tracking Environmental Change Using Lake Sediments, Volume 2: Physical and Geochemical Methods, edited by: Last, W. M. and Smol, J. P., Developments in Paleoenvironmental Research, Kluwer Academic Publishers, Dordrecht, the Netherlands, 239–269, https://doi.org/10.1007/0-306-47670-3_9, 2001.

Newell, S. E., McCarthy, M. J., Gardner, W. S., and Fulweiler, R. W.: Sediment nitrogen fixation: a call for re-evaluating coastal N budgets, Estuar. Coast., 39, 1626–1638, https://doi.org/10.1007/s12237-016-0116-y, 2016.

Nielsen, L. P.: Denitrification in sediment determined from nitrogen isotope pairing, FEMS Microbiol. Ecol., 86, 357–362, https://doi.org/10.1111/j.1574-6968.1992.tb04828.x, 1992.

Nizzoli, D., Carraro, E., Nigro, V., and Viaroli, P.: Effect of organic enrichment and thermal regime on denitrification and dissimilatory nitrate reduction to ammonium (DNRA) in hypolimnetic sediments of two lowland lakes, Water Res., 44, 2715–2724, https://doi.org/10.1016/j.watres.2010.02.002, 2010.

Paerl, H. W.: Role of heterotrophic bacteria in promoting N_2 fixation by *Anabaena* in aquatic habitats, Microb. Ecol., 4, 215–231, https://doi.org/10.1007/BF02015078, 1977.

Paerl, H. W. and Fulton, R. S.: Ecology of harmful cyanobacteria, in: Ecology of Harmful Algae, edited by: Granéli, E. and Turner, J. T., Ecological Studies, 189, Springer, Berlin, Heidelberg, Germany, 95–109, https://doi.org/10.1007/978-3-540-32210-8_8, 2006.

Paerl, H. W. and Huisman, J.: Blooms like it hot, Science, 320, 57–58, https://doi.org/10.1126/science.1155398, 2008.

Paerl, H. W., Fitzpatrick, M., and Bebout, B. M.: Seasonal nitrogen fixation dynamics in a marine microbial mat: potential roles of cyanobacteria and microheterotrophs, Limnol. Oceanogr., 41, 419–427, https://doi.org/10.4319/lo.1996.41.3.0419, 1996.

Paerl, H. W., Scott, J. T., McCarthy, M. J., Newell, S. E., Gardner, W. S., Havens, K. E., Hoffman, D. K., Wilhelm, S. W., and Wurtsbaugh, W. A.: It takes two to tango: when and where dual nutrient (N & P) reductions are needed to protect lakes and downstream ecosystems, Environ. Sci. Technol., 50, 10805–10813, https://doi.org/10.1021/acs.est.6b02575, 2016.

Phlips, E. J., Ihnat, J., and Conroy, M.: Nitrogen fixation by the benthic freshwater cyanobacterium *Lyngbya wollei*, Hydrobiologia, 234, 59–64, https://doi.org/10.1007/BF00010779, 1992.

https://doi.org/10.5194/egusphere-2026-6811
Preprint. Discussion started: 11 November 2026
© Author(s) 2026. CC BY 4.0 License.

Poirier-Larabie, S., Hudon, C., Poirier Richard, H.-P., and Gagnon, C.: Cyanotoxin release from the benthic, mat-forming cyanobacterium *Microseira* (*Lyngbya*) *wollei* in the St. Lawrence River, Canada, Environ. Sci. Pollut. R., 27, 30285–30294, https://doi.org/10.1007/s11356-020-09290-2, 2020.

Powell, M. E. and McCoy, S. J.: Divide and conquer: spatial and temporal resource partitioning structures benthic cyanobacterial mats, J. Phycol., 60, 254–272, https://doi.org/10.1111/jpy.13443, 2024.

Putnam, S. P., Smith, M. L., Metz, T. T., Womer, A. M., Sellers, E. J., McClain, S. J., Crandell, C. A., Scott, G. I., Shaw, T. J., and Ferry, J. L.: Growth of the harmful benthic cyanobacterium *Microseira wollei* is driven by legacy sedimentary phosphorous, Harmful Algae, 117, 102263, https://doi.org/10.1016/j.hal.2022.102263, 2022.

R Core Team: R: A language and environment for statistical computing, R Foundation for Statistical Computing, Vienna, Austria, https://www.R-project.org/ (last access: 23 September 2026), 2024.

Rahman, M. M., Roberts, K. L., Grace, M. R., Kessler, A. J., and Cook, P. L. M.: Role of organic carbon, nitrate and ferrous iron on the partitioning between denitrification and DNRA in constructed stormwater urban wetlands, Sci. Total Environ., 666, 608–617, https://doi.org/10.1016/j.scitotenv.2019.02.225, 2019.

Rahman, M. M., Peipoch, M., Kan, J., Sena, M., Joshi, B., Dwivedi, D., Gold, A. J., Groffman, P. M., Galella, J. G., and Inamdar, S.: Dissimilatory nitrate reduction to ammonium (DNRA) can undermine nitrogen removal effectiveness of persistently reducing riparian sediments, ACS ES&T Water, 4, 3873–3881, https://doi.org/10.1021/acsestwater.4c00185, 2024.

Rao, A. M. F. and Charette, M. A.: Benthic nitrogen fixation in an eutrophic estuary affected by groundwater discharge, J. Coastal Res., 28, 477–485, https://doi.org/10.2112/JCOASTRES-D-11-00057.1, 2012.

Reed, M. H., Strope, E. K., Cremona, F., Myers, J. A., Newell, S. E., and McCarthy, M. J.: Effects of filtration timing and pore size on measured nutrient concentrations in environmental water samples, Limnol. Oceanogr.-Meth., 21, 1–12, https://doi.org/10.1002/lom3.10529, 2023.

Risgaard-Petersen, N. and Rysgaard, S.: Nitrate reduction in sediments and waterlogged soil measured by ^{15}N techniques, in: Methods in Applied Soil Microbiology and Biochemistry, edited by: Alef, K. and Nannipieri, P., Academic Press, London, 287–295, 1995.

Risgaard-Petersen, N., Nielsen, L. P., Rysgaard, S., Dalsgaard, T., and Meyer, R. L.: Application of the isotope pairing technique in sediments where anammox and denitrification coexist, Limnol. Oceanogr.-Meth., 1, 63–73, https://doi.org/10.4319/lom.2003.1.63, 2003.

https://doi.org/10.5194/egusphere-2026-6811
Preprint. Discussion started: 11 November 2026
© Author(s) 2026. CC BY 4.0 License.

992 Robertson, E. K. and Thamdrup, B.: The fate of nitrogen is linked to iron(II) availability in a
993 freshwater lake sediment, Geochim. Cosmochim. Ac., 205, 84–99,
994 https://doi.org/10.1016/j.gca.2017.02.014, 2017.

995 Scott, J. T. and McCarthy, M. J.: Nitrogen fixation may not balance the nitrogen pool in lakes
996 over timescales relevant to eutrophication management, Limnol. Oceanogr., 55, 1265–
997 1270, https://doi.org/10.4319/lo.2010.55.3.1265, 2010.

998 Scott, J. T., McCarthy, M. J., Gardner, W. S., and Doyle, R. D.: Denitrification, dissimilatory
999 nitrate reduction to ammonium, and nitrogen fixation along a nitrate concentration gradient
1000 in a created freshwater wetland, Biogeochemistry, 87, 99–111,
1001 https://doi.org/10.1007/s10533-007-9171-6, 2008.

1002 Scott, J. T., Taylor, J. M., Andersen, I. M., Hoke, A. K., and Kelly, P. T.: Reducing nitrogen
1003 inputs can rapidly reverse eutrophication in shallow phosphorus-rich lakes, Environ. Sci.
1004 Technol., 59, 22576–22586, https://doi.org/10.1021/acs.est.5c05392, 2025.

1005 Seeberg-Elverfeldt, J., Schlüter, M., Feseker, T., and Kölling, M.: Rhizon sampling of
1006 porewaters near the sediment-water interface of aquatic systems, Limnol. Oceanogr.-
1007 Meth., 3, 361–371, https://doi.org/10.4319/lom.2005.3.361, 2005.

1008 Seitzinger, S. P.: Denitrification in freshwater and coastal marine ecosystems: ecological and
1009 geochemical significance, Limnol. Oceanogr., 33, 702–724,
1010 https://doi.org/10.4319/lo.1988.33.4part2.0702, 1988.

1011 Smolders, E., Baetens, E., Verbeeck, M., Nawara, S., Diels, J., Verdievel, M., Peeters, B., De
1012 Cooman, W., and Baken, S.: Internal loading and redox cycling of sediment iron explain
1013 reactive phosphorus concentrations in lowland rivers, Environ. Sci. Technol., 51, 2584–
1014 2592, https://doi.org/10.1021/acs.est.6b04337, 2017.

1015 Song, G. D., Liu, S. M., Kuypers, M. M. M., and Lavik, G.: Application of the isotope pairing
1016 technique in sediments where anammox, denitrification, and dissimilatory nitrate reduction
1017 to ammonium coexist, Limnol. Oceanogr.-Meth., 14, 801–815,
1018 https://doi.org/10.1002/lom3.10127, 2016.

1019 Souza, V. F., Santoro, A. L., van Weerelt, M., and Enrich-Prast, A.: Sediment denitrification,
1020 DNRA and anammox rates in tropical floodplain lake (Pantanal, Brazil), Oecol. Aust., 16,
1021 734–744, https://doi.org/10.4257/oeco.2012.1604.01, 2012.

1022 Stachelek, J., Ford, C., Kincaid, D., King, K., Miller, H., and Nagelkirk, R.: The National
1023 Eutrophication Survey: lake characteristics and historical nutrient concentrations, Earth
1024 Syst. Sci. Data, 10, 81–86, https://doi.org/10.5194/essd-10-81-2018, 2018.

1025 Stal, L. J.: Nitrogen fixation in cyanobacterial mats, Method. Enzymol., 167, 474–484,
1026 https://doi.org/10.1016/0076-6879(88)67052-2, 1988.

https://doi.org/10.5194/egusphere-2026-6811
Preprint. Discussion started: 11 November 2026
© Author(s) 2026. CC BY 4.0 License.



Stal, L. J.: Physiological ecology of cyanobacteria in microbial mats and other communities, New Phytol., 131, 1–32, https://doi.org/10.1111/j.1469-8137.1995.tb03051.x, 1995.

Stevenson, R. J., Pinowska, A., Albertin, A., and Sickman, J. O.: Ecological condition of algae and nutrients in Florida springs: the synthesis report, Florida Department of Environmental Protection, Tallahassee, FL, USA, 2007.

Tian, L., Jiang, H., Bai, L., Wang, C., and Xu, S.: Biological nitrogen fixation in sediments of a cyanobacterial bloom-occurring bay in one eutrophic shallow lake: occurrence and related environmental factors, J. Geophys. Res.-Biogeo., 126, e2021JG006342, https://doi.org/10.1029/2021JG006342, 2021.

Tiedje, J. M.: Ecology of denitrification and dissimilatory nitrate reduction to ammonium, in: Biology of Anaerobic Microorganisms, edited by: Zehnder, A. J. B., John Wiley & Sons, New York, USA, 179–244, 1988.

Tiedje, J. M., Sexstone, A. J., Myrold, D. D., and Robinson, J. A.: Denitrification: ecological niches, competition and survival, Antonie van Leeuwenhoek, 48, 569–583, https://doi.org/10.1007/BF00399542, 1983.

Tufford, D., Kloot, R., Shea, A., McGee, S., Porter, D., Foote, D., Hankinson, W., and Donelan, T.: Water quality monitoring and research at Lake Wateree, SC, in: Proceedings of the 2012 South Carolina Water Resources Conference, Columbia, SC, USA, 10–11 October 2012, https://open.clemson.edu/cgi/viewcontent.cgi?article=1079&context=scwrc (last access: 24 October 2026), 2012.

Ullman, W. J. and Aller, R. C.: Diffusion coefficients in nearshore marine sediments, Limnol. Oceanogr., 27, 552–556, https://doi.org/10.4319/lo.1982.27.3.0552, 1982.

Vadeboncoeur, Y., Vander Zanden, M. J., and Lodge, D. M.: Putting the lake back together: reintegrating benthic pathways into lake food web models, BioScience, 52, 44–54, https://doi.org/10.1641/0006-3568(2002)052[0044:PTLBTR]2.0.CO;2, 2002.

Vadeboncoeur, Y., Jeppesen, E., Vander Zanden, M. J., Schierup, H.-H., Christoffersen, K., and Lodge, D. M.: From Greenland to green lakes: cultural eutrophication and the loss of benthic pathways in lakes, Limnol. Oceanogr., 48, 1408–1418, https://doi.org/10.4319/lo.2003.48.4.1408, 2003.

Venkatachari, A., Bourbonnais, A., and Cottingham, K. L.: Data for "Benthic cyanobacterial mats enhance nitrogen turnover in a eutrophic reservoir", OSF [data set], https://doi.org/10.17605/OSF.IO/D98XZ, 2025.

WaterWatch: 2024 Water Watch Annual Report, Lake Wateree Association, https://drive.google.com/file/d/1yI68-fzF1MmkSCEYI9xAG5nkbtR8M0S5/view (last access: 12 August 2025), 2025.

https://doi.org/10.5194/egusphere-2026-6811
Preprint. Discussion started: 11 November 2026
© Author(s) 2026. CC BY 4.0 License.

Wood, S. A., Kelly, L. T., Bouma-Gregson, K., Humbert, J.-F., Laughinghouse IV, H. D., Lazorchak, J., McAllister, T. G., McQueen, A., Pokrzywinski, K., Puddick, J., Quiblier, C., Reitz, L. A., Ryan, K. G., Vadeboncoeur, Y., Zastepa, A., and Davis, T. W.: Toxic benthic freshwater cyanobacterial proliferations: challenges and solutions for enhancing knowledge and improving monitoring and mitigation, Freshwater Biol., 65, 1824–1842, https://doi.org/10.1111/fwb.13532, 2020.

Wurtsbaugh, W. A., Paerl, H. W., and Dodds, W. K.: Nutrients, eutrophication and harmful algal blooms along the freshwater to marine continuum, WIREs Water, 6, e1373, https://doi.org/10.1002/wat2.1373, 2019.

Yang, L., Cao, X.-Y., Chen, X.-Y., Deng, Q.-H., Wan, L.-L., Li, X.-W., Zhou, Y.-Y., and Song, C.-L.: Community composition and functional genes explain different ecological roles of heterotrophic bacteria attached to two bloom-forming cyanobacterial genera, Sci. Total Environ., 758, 143850, https://doi.org/10.1016/j.scitotenv.2020.143850, 2021.

Ye, L., Xiao, Y., Qin, J., Tang, J., Yin, Y., and Zhang, W.: The influence of redox potential on phosphorus release from sediments in different water bodies, Mar. Pollut. Bull., 207, 116909, https://doi.org/10.1016/j.marpolbul.2024.116909, 2024.

Yin, G., Hou, L., Liu, M., Liu, Z., and Gardner, W. S.: A novel membrane inlet mass spectrometer method to measure $^{15}NH_4^+$ for isotope-enrichment experiments in aquatic ecosystems, Environ. Sci. Technol., 48, 9555–9562, https://doi.org/10.1021/es501261s, 2014.

Yin, Q., Carmichael, W. W., and Evans, W. R.: Factors influencing growth and toxin production by cultures of the freshwater cyanobacterium *Lyngbya wollei* Farlow ex Gomont, J. Appl. Phycol., 9, 55–63, https://doi.org/10.1023/A:1007959002191, 1997.

Yoshinaga, I., Amano, T., Yamagishi, T., Okada, K., Ueda, S., Sako, Y., and Suwa, Y.: Distribution and diversity of anaerobic ammonium oxidation (anammox) bacteria in the sediment of a eutrophic freshwater lake, Lake Kitaura, Japan, Microbes Environ., 26, 189–197, https://doi.org/10.1264/jsme2.ME10184, 2011.

Yuan, H., Jia, B., Zeng, Q., Zhou, Y., Wu, J., Wang, H., Fang, H., Cai, Y., and Li, Q.: Dissimilatory nitrate reduction to ammonium (DNRA) potentially facilitates the accumulation of phosphorus in lake water from sediment, Chemosphere, 303, 134664, https://doi.org/10.1016/j.chemosphere.2022.134664, 2022.

Zhang, D., Li, M., Yang, Y., Yu, H., Xiao, F., Mao, C., Huang, J., Yu, Y., Wang, Y., Wu, B., Wang, C., Shu, L., He, Z., and Yan, Q.: Nitrite and nitrate reduction drive sediment microbial nitrogen cycling in a eutrophic lake, Water Res., 220, 118637, https://doi.org/10.1016/j.watres.2022.118637, 2022.

Zhu, L., Shi, W., Van Dam, B., Kong, L., Yu, J., and Qin, B.: Algal accumulation decreases sediment nitrogen removal by uncoupling nitrification-denitrification in shallow eutrophic

https://doi.org/10.5194/egusphere-2026-6811
Preprint. Discussion started: 11 November 2026
© Author(s) 2026. CC BY 4.0 License.



1099 lakes, Environ. Sci. Technol., 54, 6194–6201, https://doi.org/10.1021/acs.est.9b05549,
1100 2020.